Self-consistent electron energy distribution functions, vibrational distributions, electronic excited state kinetics in reacting microwave CO_2 plasma: An advanced model ⊕

L. D. Pietanza ✉ ; G. Colonna ; M. Capitelli

Check for updates

CrossMark

View Online

Export Citation

Articles You May Be Interested In

User Evaluation of 3D-Printed Personalized Saxophone Mouthpieces

Proc. Mtgs. Acoust (September 2022)

Characterizing the soundscape of tranquil urban spaces

Proc. Mtgs. Acoust (June 2013)

Acoustics education in the Low Countries

J Acoust Soc Am (February 1999)

Physics of Plasmas

Physics of Plasmas

Features in Plasma Physics Webinars

Register Today!

AIP Publishing

Self-consistent electron energy distribution functions, vibrational distributions, electronic excited state kinetics in reacting microwave CO$_2$ plasma: An advanced model (EP)

View Online   Export Citation   CrossMark

L. D. Pietanza,[a] (iD) G. Colonna, (iD) and M. Capitelli (iD)

AFFILIATIONS

CNR-ISTP, Istituto per la Scienza e Tecnologia dei Plasmi, sez. Bari (Italy) Via Amendola 122/D, 70126 Bari, Italy

[a] Author to whom correspondence should be addressed: luciadaniela.pietanza@cnr.it

ABSTRACT

An advanced model for the calculation of electron energy distribution functions (eedfs), vibrational distributions, and electronic excited state densities of reacting CO$_2$ in microwave (MW) discharges has been developed for clarifying: (1) the role of electronic states of the relevant neutral species in affecting the eedf and (2) the contribution to the CO$_2$ dissociation of the electron impact and heavy particle dissociation mechanisms. To model the discharge, the power density typical of MW discharges is used as a parameter. Different case studies including optically thick and thin plasmas and the dependence of the CO$_2$ dissociation rates on the gas temperature are investigated. The results show that at a low gas temperature, i.e., 300 K, the heavy-particle dissociation mechanism, also called the pure vibrational mechanism, prevails on the electron impact dissociation one, while at a high gas temperature, i.e., 2000 K, the two mechanisms become competitive and the global behavior strongly depends on the choice of electron impact dissociation cross sections. Large differences appear in the eedf, especially in the post-discharge regime, when considering thick and thin plasmas. In the thick case, a well-structured eedf appears as a result of superelastic collisions mainly involving the electronic states of the relevant neutral species. In the thin plasma, many peaks disappear because the concentration of the excited states strongly decreases. Finally, our model gives the results of conversion and energy efficiency as well as vibrational distributions in satisfactory agreement with the corresponding results calculated by the Antwerp group.

I. INTRODUCTION

A large amount of interest is presently devoted to the application of the state-to-state (STS) plasma kinetics self-consistently coupled to a suitable Boltzmann equation (BE) for the electron energy distribution function (eedf) in plasmas of different nature. The method, which has a long history started many years ago, was able to understand (1) the plasma kinetics of H$_2$ for the formation of negative ions;[1,2] (2) the microwave plasmas used for the formation of diamond films;[3] and (3) the kinetics of diatomic molecules (H$_2$,[4,5] N$_2$,[6] and O$_2$[7]) for different applications. Many other cases including laser kinetics, hypersonic flows, and boundary layer kinetics have been reported elsewhere.[8,9]

The understanding of the activation of CO$_2$ by cold plasmas in different conditions, i.e., microwave (MW), dielectric barrier discharge (DBD), nanopulsed discharges (ND), etc., is probably the major problem in this topic, intensively investigated in the last few years. Many experimental studies are being conducted with the aim to reach the

values of CO$_2$ dissociation rates obtained by Fridman[10] under microwave conditions. On the other hand, large theoretical efforts are being developed by different teams to better understand the electrical conditions necessary for maximizing the dissociation process of CO$_2$.

In particular, Kozák and Bogaerts,[11,12] Bogaerts et al.,[13] and Aerts et al.[14] developed an interesting plasma chemistry model with particular attention to the vibrational kinetics of CO$_2$ to better understand the role of vibrational assisted dissociation processes in the activation of CO$_2$. Important experimental and theoretical contributions have been presented by their group obtaining a satisfactory agreement between model prediction and experimental results. Less attention was dedicated to the eedf of the system, obtained, in any case, by solving a Boltzmann equation code.

On the other hand, Pietanza et al.,[15] Capitelli et al.,[16] and Capitelli et al.[17] focused their efforts to develop a self-consistent model for CO$_2$ plasmas, coupling the Boltzmann equation for eedf and

plasma kinetics, and describing the vibrational and the electronic excited states kinetics under discharge and post discharge conditions.

The first approach was to solve a Boltzmann equation for the eedf by considering the concentration of excited states as parameters.[18,19] In particular, a Boltzmann distribution of vibrationally excited states for both symmetric and asymmetric CO_2 modes characterized by parametric vibrational temperatures was inserted in the Boltzmann equation code. In addition, the metastable electronic excited state of CO_2 at 10.5 eV was also considered in the Boltzmann equation and described with the parametric concentrations. The corresponding results showed the importance of superelastic vibrational and electronic collisions in affecting the eedf under discharge and afterglow conditions. In particular, superelastic vibrational collisions were responsible for the increase of the eedf with the vibrational temperatures, while the superelastic electronic collisions, instead, created characteristic peaks in the eedf at 10.5 eV in the post-discharge, whose height was proportional to the concentration of the 10.5 eV CO_2 state.

As a further step, the Boltzmann equation was solved self-consistently with the vibrational and electronic kinetics by considering plasma conditions where the dissociation of CO_2 was small to avoid the complication of the formed products, CO and O atoms, in affecting the eedf and the different vibrational distribution functions (vdfs).[15–17] Interesting results were obtained in these studies qualitatively confirming the parametric results in Refs. 18 and 19. It was stressed in the conclusions of these papers the importance to insert in the plasma kinetics of pure CO_2 a corresponding kinetics for the reaction products (CO and O), as well as for the molecular oxygen formed by the recombination process of O atoms.

In this context, sophisticated plasma kinetics for reacting CO[20–22] was developed. The main results concerned the role of the electronically excited states of CO in structuring the eedf in the post discharge regime. Optically thin and thick plasmas as well as some important quenching processes of CO metastable electronic states were considered. Optically thin and thick plasmas were also considered by D'Ammando et al.[23] in H_2/He plasma. The corresponding kinetics was then enriched by the presence of oxygen and carbon atoms formed, respectively, by the direct dissociation of CO and by the Boudouard reaction.

In the present work, we present, for the first time, the results obtained by solving self-consistently the Boltzmann equation for reacting CO_2, in which besides the kinetics of CO_2, also the kinetics of the CO_2 dissociation products such as CO, O, and C are taken into account both in the plasma chemistry and in the electron Boltzmann equation. In this way, we can explore conditions in which CO_2 dissociation is more important than those presented in our previous studies,[15–17] increasing the power density of the discharge and/or extending the discharge pulse duration. In addition, in the present work, we also insert the presence of molecular oxygen (O_2) coming from the recombination of atomic oxygen.

Contrary to our previous studies, during the pulse discharge, instead of E/N values, we use constant values of the power density, a parameter which is often used to characterize experimental conditions. The advantage of using a constant power density is to stabilize our code allowing to extend the pulse discharge residence times.

The CO_2 dissociation model used is based on two important dissociation channels: the direct electron impact mechanism (DEM), described by an opportune electron impact dissociation cross section,

i.e., the Hake and Phelps one with an energy threshold of 7 eV or the experimental Cosby and Helm one with a threshold of 11.6 eV, and the pure vibrational mechanism (PVM), i.e., the dissociation induced by vibrational excitation with a threshold of 5.5 eV. The latter channel is described by vibrational state resolved heavy particle dissociation collisions characterized by global Arrhenius rate coefficients with specific activation energies. This model is independent from the explicit shape of the electronic excited states potential energy curves of CO_2 electronic excited states, in particular of the ${}^1B_2$ and ${}^3B_2$ states, which do not enter as specific states in our model. In the future, more exact potential energy curve calculations could clarify the complex energy diagram of the CO_2 system close to the effective dissociation limit and prepare a more refined dissociation model.

The aim of this work is to: (1) show the role of electronically excited states of CO, O_2, O, and C in affecting the eedf for reacting CO_2 for optically thick and thin plasmas; (2) show the role of non equilibrium vibrational distributions of CO_2, CO, and O_2 in affecting the PVM rates of CO_2 and CO and compare them with the corresponding DEM ones; (3) compare our results with the corresponding ones from Kozák and Bogaerts[11] and Berthelot and Bogaerts;[24] (4) investigate the effect of gas temperature and of the electron impact dissociation cross section choice on the CO_2 dissociation; and (5) show the perspectives to increase the accuracy of the dissociation process of CO_2 in MW discharges.

The paper is divided in five sections. After the introduction, Sec. II briefly describes the plasma kinetics focusing on the energy level diagrams of the different species (Sec. II A); the electron impact cross sections (Sec. II B); the heavy particle chemistry (Sec. II C); and the vibrational and electronic excited state kinetic models (Sec. II D). Section III describes the results including a MW test case at a low gas temperature in the optically thick plasma (Sec. III A), the same test case in the optically thin plasma (Sec. III B), the dissociation rates for CO_2 and CO (Sec. III C), the conversion and energy efficiency (Sec. III D) at different power densities, and the investigation of the gas temperature role in affecting CO_2 dissociation (Sec. III E). Conclusions and perspectives are reported in Sec. IV, while the list of all the level species and kinetic processes inserted into the model are displayed in the tables reported in the Appendix.

II. PLASMA KINETICS

The plasma kinetics is described by using a 0D time dependent selfconsistent model in which the electron Boltzmann equation is solved simultaneously and selfconsistently with the non-equilibrium STS vibrational kinetics of the plasma heavy particles, the kinetic of the electronically excited states, and a simplified plasma chemistry model, which takes into account the most relevant chemical processes such as dissociation/recombination and ionization/recombination.

Our model calculates simultaneously the time evolution of the eedf, the vdfs of the molecules, the electronic excited state population densities, and the plasma composition, according to the relevant kinetic processes accounted in the model. Different conditions similar to the ones characterizing MW, DBD, and NRP plasma discharges can be investigated both in discharge and post-discharge conditions by choosing opportunely the gas temperature, the pressure, the reduced electric field, and/or the power density of the discharge and the discharge residence time.

In the present contribution, we will focus on the description of MW plasma discharges due to their importance for the CO_2 plasma

assisted dissociation, providing the highest CO_2 conversion rates with the highest energy efficiencies.

The model has been applied to a CO_2 reacting plasma with the following species: CO_2, CO, O_2, C, O, CO_2^+, CO^+, O_2^+, C^+, O^+, O^-, and e^-.

A. Energy level diagrams

The energy level diagrams of the neutral species (CO_2, CO, O_2, C, and O) are represented in Fig. 1.

All the vibrational and electronic excited states included into the model are listed in Tables II and III of the Appendix.

In particular, for the CO_2 ground electronic state ($X^1\Sigma_g^+$), all the pure asymmetric levels of the kind $(00v)$ up to the dissociation limit of $5.5\,eV$, i.e., 21 levels, are taken into account together with the first bending mode $v_{b_1}(010)$ and three Fermi levels, i.e., $v_{FL_1}(020) + (100)$, $v_{FL_2}(030) + (110)$, and $v_{FL_3}(040) + (120) + (200)$. Only one CO_2 electronic excited state at $10.5\,eV$ is accounted for into the model. In the bulk of the results, this state is considered as a metastable state, strongly affecting the eedf through the corresponding superelastic electronic collisions. Important effects on the eedf are also obtained if this state is considered as a dissociative state (see Sec. III B).

For CO, 80 vibrational levels in the ground electronic excited state ($X^1\Sigma^+$) and seven electronic excited states, three triplets and four singlets, are taken into account.

For O_2, instead, 34 vibrational levels are accounted in the ground electronic excited state ($X^3\Sigma_g^-$) and two low lying electronic levels ($a^1\Delta_g$ and $b^1\Sigma_g^+$).

Several low lying electronic excited states are accounted also for O and C atoms, while ions are considered only in their ground electronic state.

B. Electron impact cross sections

The electron impact cross sections involved in the electron Boltzmann equation are listed in Table IV of the Appendix.

For CO_2, the cross sections have been essentially taken from the Hake and Phelps database[25] which provides excitation from the ground state for the first bending level and the three low lying Fermi levels (X2 in Table IV), the first asymmetric level and the electronic excited state at $10.5\,eV$ (X4 in Table IV), and ionization and dissociation cross sections. In addition to the Hake and Phelps dissociation cross section with threshold energy $7\,eV$, different choices for this cross section can also be as reported in Refs. 26 and 27, in particular the experimental Cosby and Helm one[28] with threshold energy $11.6\,eV$. The cross sections for vibrational excitation (e–V), dissociation, and ionization are available only for the ground state and scaling laws are used to extend them to higher vibrational levels. In particular, the Fridman scaling law[10] is used for the vibrational excitation of pure asymmetric levels (X3 in Table IV), i.e.,

$$\sigma_{vw}(\varepsilon) = \exp\left(\frac{-\alpha(\omega - v - 1)}{1 + \beta v}\right)\sigma_{01}(\varepsilon + E_{01} - E_{vw}). \qquad (1)$$

According to Eq. (1), the cross section for transitions involving higher vibrational levels $(00v) \rightarrow (00\omega)$ can be calculated from the cross
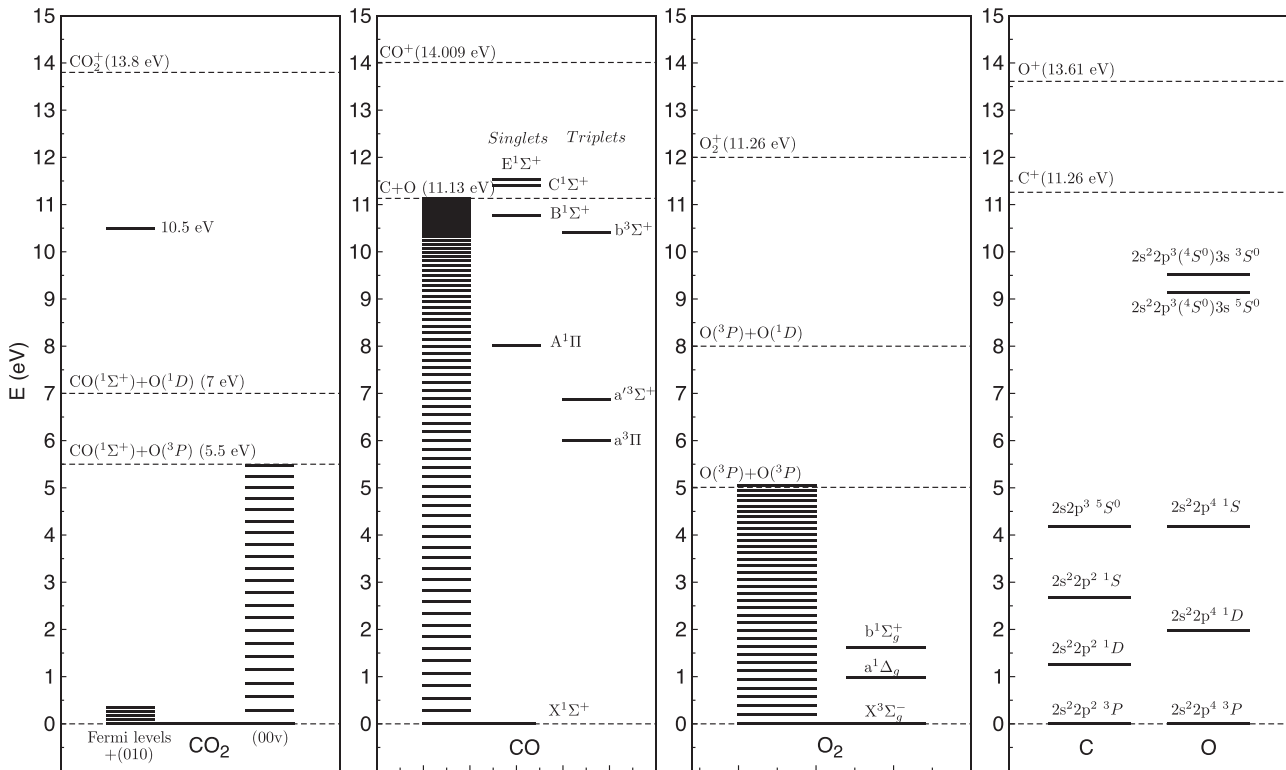

FIG. 1. Energy level diagrams for CO_2, CO, O_2, C, and O.

section σ_{01} of the transition $(000) \to (001)$ with threshold E_{01} by shifting it on the energy scale by the threshold energy E_{vw} and by scaling its magnitude according to two parameters ($\alpha = 0.5$ and $\beta = 0.0$, for the asymmetric mode levels[10]).

For dissociation and ionization cross sections from higher vibrational levels v (X5 and X6 in Table IV), a simple threshold shifting by the vibrational level E_v is applied to the ground state cross section σ_0 with threshold E_0

$$\sigma_v(\varepsilon) = \sigma_0(\varepsilon + E_0 - E_v). \tag{2}$$

For the CO system, the cross sections have been taken from the Itikawa database[29] which provides momentum transfer (X7 in Table IV), ionization cross section from the ground state (X13 in Table IV), and excitation cross sections from the ground state of the several electronic excited states introduced into the model (X14 in Table IV). For direct dissociation cross section (X15 in Table IV), the experimental Cosby cross section (threshold 13.5 eV) is used.[30] To obtain vibrational state resolved ionization and dissociation cross sections for CO (X13 and X15 in Table IV), the same threshold shifting used for CO_2 is used [see Eq. (2)]. New resonant vibrational state resolved electron impact cross sections have been taken into account for CO, in particular vibrational excitation (X8 in Table IV),[31] resonant dissociation (X9 in Table IV),[32] and dissociative electron attachment (X10 in Table IV)[32] cross sections. These resonant cross sections are in general small for lower vibrational levels but increase rapidly for higher vibrational levels thus increasing their importance in conditions of high vibrational excitation.

Also for the O_2 system, a complete set of vibrational state resolved resonant e–V (X17 in Table IV),[33] resonant dissociation (X18 in Table IV),[34] and resonant dissociative electron attachment (X23 in Table IV)[34] cross sections are included in the model. Direct dissociation cross sections calculated by the semiclassical approximation are also included, both for the Herzberg (only for v = 0,1,2) (X19 in Table IV)[35] and for the Schumann transitions (for $v \leq 30$) (X20 in Table IV), together with a Schumann pre-dissociation channel (for $v \leq 30$) (X21 in Table IV).[36] O_2 ionization cross sections for $v \leq 32$ (X22 in Table IV) are taken from Ref. 37.

C. Heavy-particle chemistry

Several heavy-particle chemical processes described by Arrhenius rate coefficients are included in the model (see Table V in the Appendix).

For CO_2, two PVM dissociation processes are accounted for the asymmetric mode: the heavy particle dissociation induced by all particles (H1 in Table V) and the dissociation induced by collision with the O atom (H2 in Table V) with their reverse ones (H3 and H4 in Table V, respectively). Higher vibrational level rate coefficients (k_R) are calculated from the Arrhenius rate coefficients for transition from the ground state (k_{R0}) by using the Fridman–Macheret α-model,[10] i.e.,

$$k_R(E_v, T_{gas}) = k_{R0}\exp\left(-\frac{E_a - \alpha E_v}{T_{gas}}\right), \tag{3}$$

where E_a is the activation energy, E_v is the vibrational energy, and α is the Fridman–Macheret coefficient.

According to this model, the vibrational energy lowers the activation energy of the chemical reactions, greatly enhancing the corresponding rate coefficients. The α parameter entering Eq. (3) determines the efficiency of lowering the reaction barrier by the vibrational excitation and, in general, it is close to 1 for strongly endothermic reactions and close to zero for exothermic ones. The CO_2 dissociation through Eq. (3) is strongly affected by the choice of α and as a consequence also the vdf.

For CO, we take into account two different kinds of PVM dissociations. The first is direct dissociation by all particles forming C and O atoms (H6 in Table V). The other mechanism is called the Boudouard or disproportioning process in which two vibrational excited CO molecules dissociate forming a CO_2 molecule and C (H7 in Table V). For the Boudouard reaction, we use an activation energy of 8.3 eV, recently calculated by Barreto et al.,[38] by a quantum approach. This value is intermediate between the previous experimental and theoretical estimations performed by Rusanov and Fridman[39] ($E_a = 6$ eV) and by Essenigh et al.[40] ($E_a = 11.6$ eV).

For O_2, dissociation induced by collisions with O atoms and O_2 molecules are accounted with their reverse processes (H10–H11 in Table V).

O_2–O_2 dissociation and recombination have been calculated by the ladder climbing model as reported by Cacciatore et al.[41]

D. Vibrational and electronic excited state kinetic models

The vibrational kinetic processes accounted into the model are listed in Table VI in the Appendix.

For CO_2, we have included low vibrational level transitions (see V1–V7) whose rate coefficients are available in the literature and starting from them, following the approach of Kozák and Bogaerts[11] and by using appropriate scaling laws derived by the SSH theory,[42] we have calculated rate coefficients involving all the asymmetric mode levels up to the dissociation limit for the vibrational–translation (V–T) (V8 in Table VI) processes, the intramode (V–V) vibrational–vibrational (V9 in Table VI) processes, and the intermode (V–V′) vibrational–vibrational transitions (V10 in Table VI) with the symmetric mode level processes.

For CO, V–V (V12 in Table VI) and V–T (V13 in Table VI) rate coefficients have been calculated following the approach of Adamovich and Rich,[43] who have used the forced harmonic oscillator approximation (FHO) approach. The FHO theory takes into account the coupling of many vibrational states during a collision and is therefore applicable also for multi-quantum processes. A strong contribution to the CO vibrational kinetics is given by V–T deactivation due to O and C atoms (V14 and V15 in Table VI).[44] For the CO system, a very important process is the pumping of energy in the v = 27 level by quenching of the first electronic excited state of CO at 6 eV ($a^3\Pi$) (V17 in Table VI).[45]

In the present contribution, V–V transitions coupling the CO_2 and CO system (V11 Table VI) are also included.[11]

The electronic excited state kinetics is described by the following equation for the density of the ith electronic excited state (n_i):

$$\frac{dn_i}{dt} = K_{exc}^i n_e n_0 - K_{de-exc}^i n_e n_i - \sum_{j<i}\lambda_{ij}A_{ij}n_i - Q, \tag{4}$$

where K_{exc}^i and K_{de-exc}^i represent the electron impact excitation and de-excitation rate coefficients, n_e and n_0 the electron density and the

ground electronic excited state density, $\lambda_{ij}A_{ij}$ the escape factor and the Einstein coefficient for the radiative transition from the ith toward the jth electronic excited state, and Q the term due to quenching processes. All the optical transitions and the quenching channels included into the model are listed in Tables VII and VIII in the Appendix.

III. RESULTS

A. MW test case at a low gas temperature (optically thick plasma)

The following results have been obtained by applying the self-consistent model to a MW test case characterized by the following values of gas temperature, pressure, power density, pulse duration, and post-discharge time: $T_{gas} = 300$ K, P = 20 Torr, $P_d = 80$ W cm^{-3}, $t_{pulse} = 50$ ms, and $t_{pd} = 100$ ms. The Cosby electron dissociation cross section for CO_2 is used even if in some cases it is replaced by the Hake and Phelps cross section.

As an initial condition, pure CO_2 gas with an initial CO_2 molar fraction approximately equal to 1 and all the other species, including the electrons, with small molar fractions of the order of 10^{-6} is considered. Moreover, the initial vdf and eedf distributions are assumed in equilibrium at T_{gas}.

Figure 2 shows the molar fraction time evolution during the discharge (0–50 ms) and post-discharge (50–100 ms). During the discharge, CO_2 molecules dissociate forming CO and O atoms. CO also dissociates forming C and O atoms and O atoms recombine forming O_2 molecules. The electron molar fraction reaches a stationary low value of approximately 10^{-6}. In the post discharge, the electron molar fraction drops by approximately three orders of magnitude. O atoms concentration decay forming O_2, while the concentration of the main two molecules CO_2 and CO remains constant after approximately 10 ms.

Figure 3 represents the reduced electric field time evolution and the total energy density injected by the discharge in the plasma. The power density is assumed to be constant during the discharge and
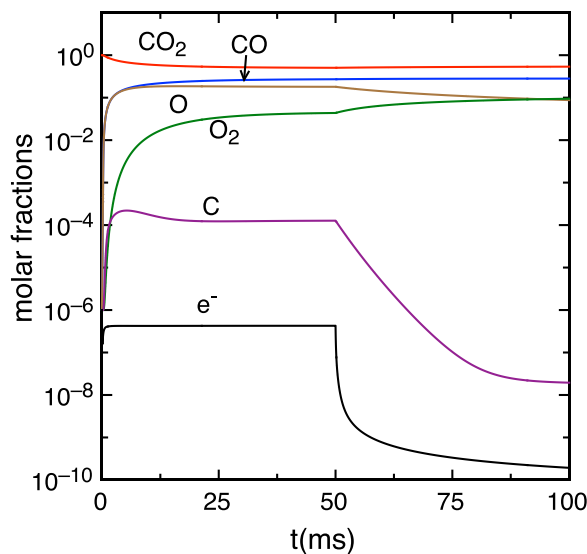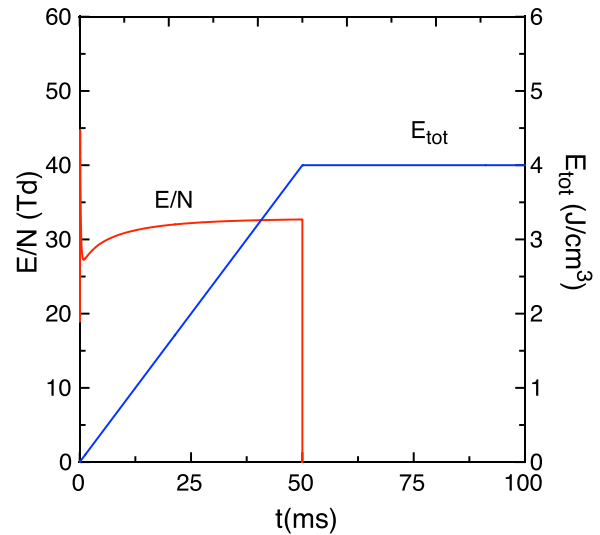

FIG. 3. Electric field and total injected energy density time evolution in the MW test case under discharge and post discharge conditions ($T_{gas} = 300$ K, P = 20 Torr, $P_d = 80$ W cm^{-3}, $t_{pulse} = 50$ ms, $t_{pd} = 100$ ms, and optically thick plasma).

since it is proportional to the electron density and to the square of the reduced electric field ($P_d \propto n_e(E/N)^2$), the reduced electric field time evolution depends on the electron density time evolution which is linked to the plasma chemistry.

Next, Fig. 4 shows the time evolution of the (a) vibrational and (b) electron temperatures. The vibrational temperatures are calculated by applying the Boltzmann distribution to the first two vibrational levels while the electron temperature is derived from the mean electron energy.

It should be noted that the vibrational temperature can be also defined through the mean vibrational energy of the system. In this case, the 0–1 vibrational temperature gives in general lower values of vibrational energy. However, this point is not important in the STS approach which treats every vibrational level as a single species so that the 0–1 vibrational temperature reported in Fig. 4(a) gives only an indication of the importance of vibrational energy in the system.

Inspection of the figure shows different vibrational temperatures for CO, CO_2, and O_2 which reflect the e–V electron processes. In particular, the low value of the O_2 vibrational temperature is due to its low value of the e–V(0–1) rates and corresponding high values of V–T $O_2(v)$-O rates. All the temperatures first increase during the discharge, after that they decrease reaching a constant value on the time scale of less than 10 ms up to 50 ms. Soon after the end of the pulse, the electron temperature drops becoming equal to the gas temperature, as well as the vibrational temperatures.

Figures 5–7 show the time evolution of the vdf of CO_2, CO, and O_2 molecules in (a) discharge and (b) post-discharge conditions. Transient and stationary vdfs are characterized by a non-equilibrium trend.

In particular, during the discharge, the vdfs are heated as a result of e–V processes, which pump energy preferentially to lower vibrational levels, and by V–V processes, which create long non-equilibrium plateaux especially in the intermediate vibrational energy range. These plateaux are depleted in the high energy part by
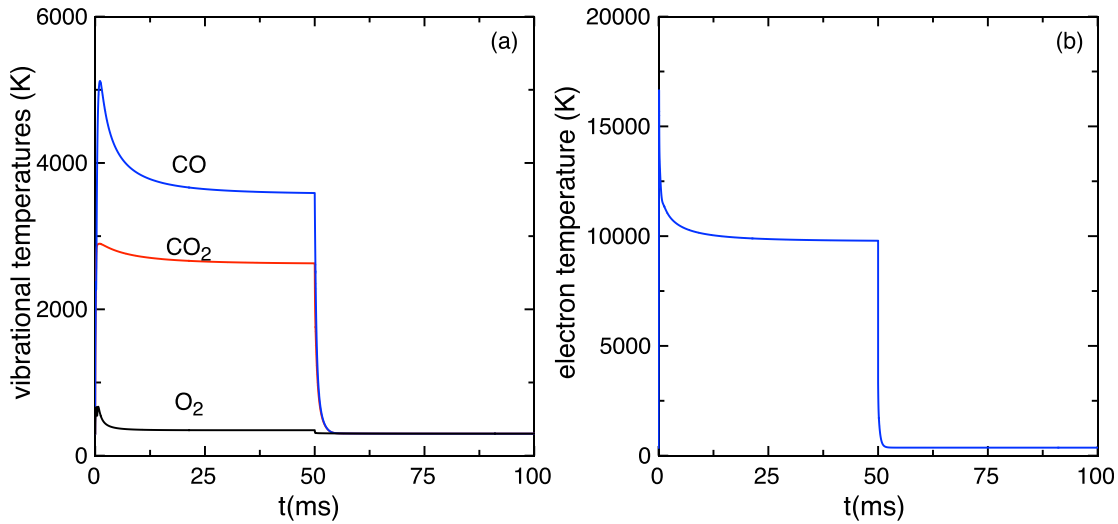

FIG. 2. Molar fraction time evolution for the MW test case under discharge and post discharge conditions ($T_{gas} = 300$ K, P = 20 Torr, $P_d = 80$ W cm^{-3}, $t_{pulse} = 50$ ms, $t_{pd} = 100$ ms, and optically thick plasma).

FIG. 4. (a) Vibrational and (b) electron temperature time evolution in the MW test case ($T_{gas} = 300$ K, $P = 20$ Torr, $P_d = 80$ W cm^{-3}, $t_{pulse} = 50$ ms, $t_{pd} = 100$ ms, and optically thick plasma).

dissociation and V–T deactivation processes. For CO_2, such depletion occurs at $v > 15$, while for CO, two depletion zones are present, the first for $v > 30$ (8.3 eV) due to the Boudouard process (H7 in Table V) and the second for $v > 60$ (10 eV) due to direct dissociation (H6 in Table V) into C and O atoms. For CO_2 and CO, the presence of over-populated vdf tails strongly enhances the dissociation channels by vibrational excitation. During the post-discharge, the vdf time evolution is dominated by V–T relaxation processes. The low energy part fast decreases reaching a Boltzmann distribution at the gas temperature but the tail of the vdfs remains in non-equilibrium.

For CO, it is evident, especially during the discharge, the presence of a peak at $v = 27$ due to the quenching process from the first electronic excited state of CO ($a^3\Pi$) at 6 eV (V17 Table VI and Q1 Table VIII). For O_2 vdf, the long plateau is essentially due to three body recombination of O atoms.

Figure 8 shows the eedf time evolution in (a) discharge and (b) post-discharge conditions. During the discharge, the eedf is driven by the electric field and by superelastic vibrational and electronic collisions of CO_2 and CO, reaching a stationary condition only at times later than 10^{-4} s. In the post-discharge, the eedf cools down fast and its shape is dominated by the peaks due to superelastic collisions involving the electronic excited states of the mixture species. For the CO_2 electronic excited state at 10.5 eV, such a process is as follows:
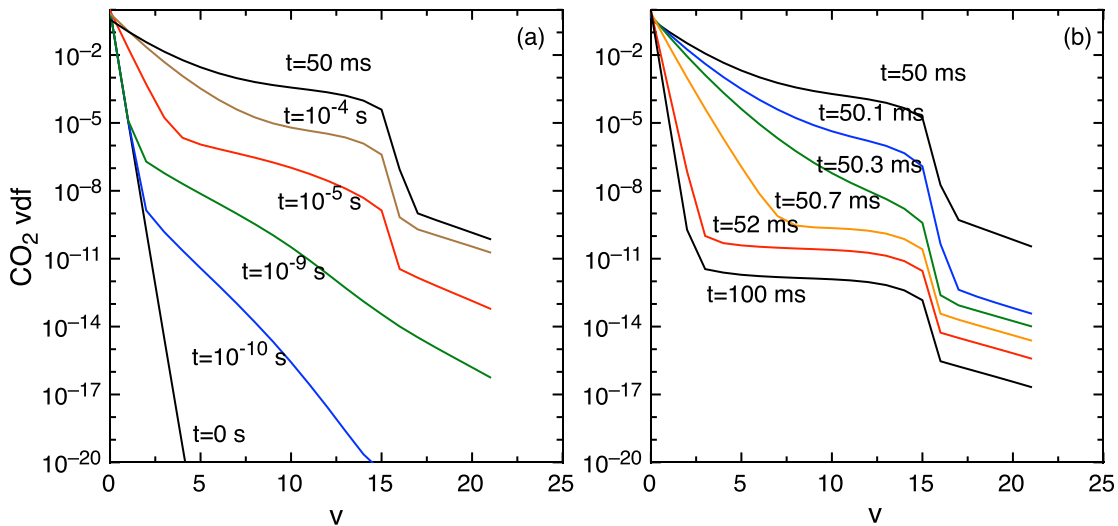

FIG. 5. CO_2 vdf time evolution in (a) discharge and (b) post-discharge in the MW test case ($T_{gas} = 300$ K, $P = 20$ Torr, $P_d = 80$ W cm^{-3}, $t_{pulse} = 50$ ms, $t_{pd} = 100$ ms, and optically thick plasma).
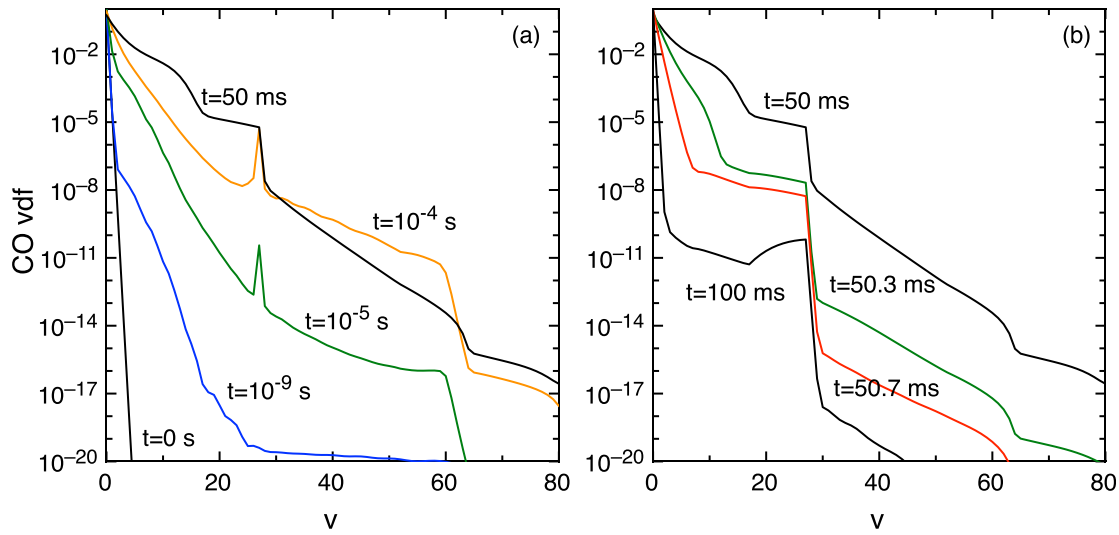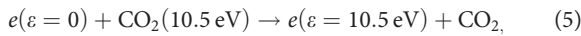
FIG. 6. CO vdf time evolution in (a) discharge and (b) post-discharge in the MW test case ($T_{gas} = 300$ K, $P = 20$ Torr, $P_d = 80$ W cm^{-3}, $t_{pulse} = 50$ ms, $t_{pd} = 100$ ms, and optically thick plasma).

$$e(\varepsilon = 0) + CO_2(10.5 \, eV) \rightarrow e(\varepsilon = 10.5 \, eV) + CO_2, \quad (5)$$

which creates a source of electrons at energy 10.5 eV.

By looking at the energy corresponding to the peaks, it is possible to understand which are the electronically excited states creating such peaks. As we can see, the eedf in the post-discharge is characterized not only by the peak due to the CO_2 electronic excited state at 10.5 eV but also by the peaks due to CO, O_2, and O atoms, in particular of $O_2(0.976 \, eV)$, $O(1.976 \, eV)$, $CO(6.863 \, eV)$, $CO(8.03 \, eV)$, $O(9.521 \, eV)$, $CO(10.4 \, eV)$, $CO(10.78 \, eV)$, $CO(11.40 \, eV)$, and $CO(11.52 \, eV)$.

The peak's height is proportional to the corresponding electronic excited state density, whose time evolution is described by Eq. (4).

B. Optically thin plasma

The non-equilibrium eedf shape is strongly dependent on the radiative and quenching processes included in the model for the electronic excited states. Next, figure (Fig. 9) shows the comparison of the eedf at the end of the discharge (t = 50 ms) and of the post-discharge (t = 100 ms) calculated in the optically thick ($\lambda_{ij} = 0$) and thin ($\lambda_{ij} = 1$) conditions and by considering the $CO_2(10.5 \, eV)$ excitation cross section as a dissociative channel (see Ref. 26).

Passing from the thick to the thin case, some differences in the eedf are observed only at the end of the post-discharge, in particular the eedf in the thin case loses all the peaks corresponding to the
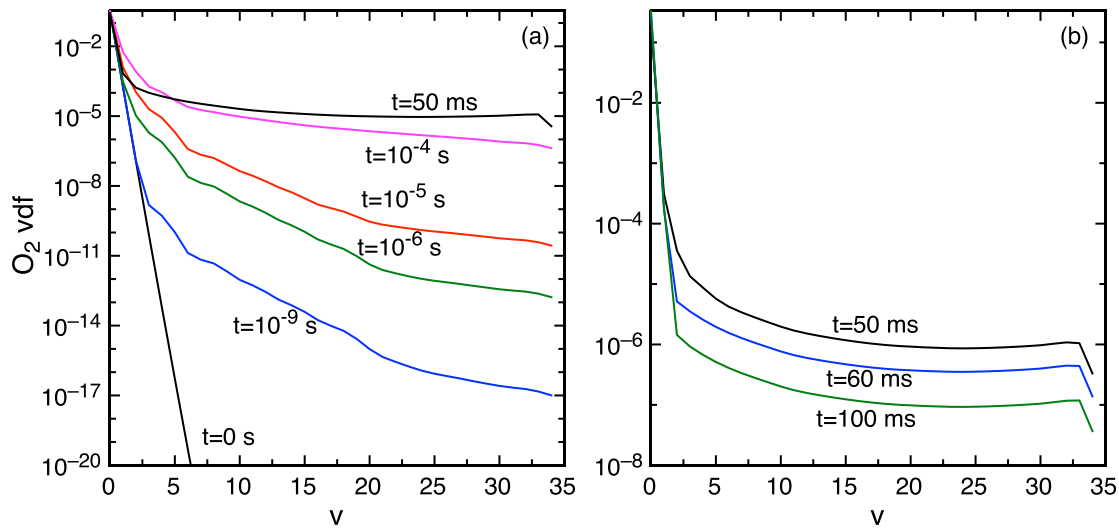

FIG. 7. O_2 vdf time evolution in (a) discharge and (b) post-discharge in the MW test case ($T_{gas} = 300$ K, $P = 20$ Torr, $P_d = 80$ W cm^{-3}, $t_{pulse} = 50$ ms, $t_{pd} = 100$ ms, and optically thick plasma).
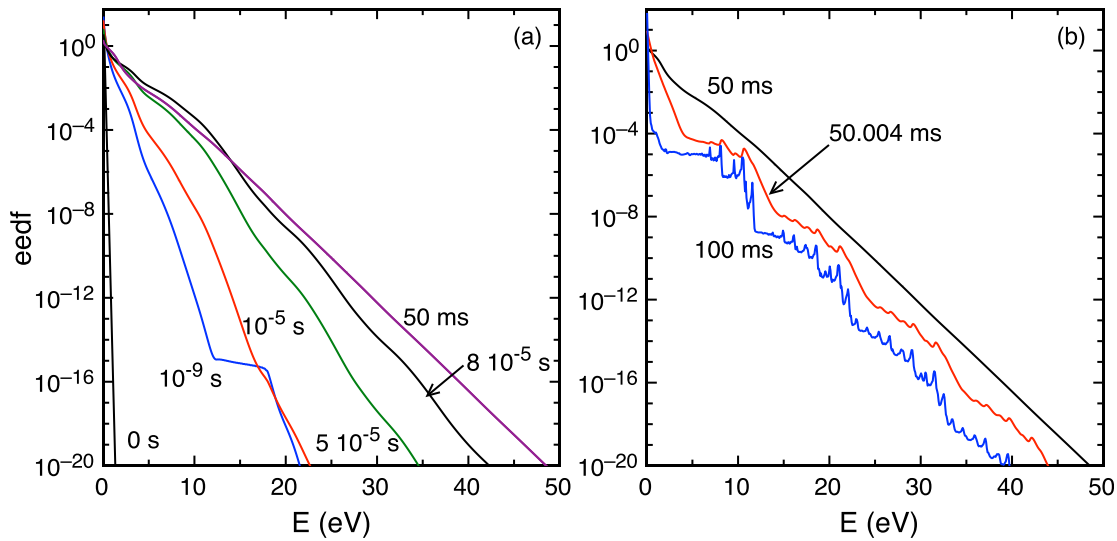
FIG. 8. Eedf time evolution in (a) discharge and (b) post-discharge in the MW test case ($T_{gas} = 300$ K, $P = 20$ Torr, $P_d = 80$ Wcm^{-3}, $t_{pulse} = 50$ ms, $t_{pd} = 100$ ms, and optically thick plasma).

emitting electronic excited states (see Table VII in Appendix), with the only exception of the CO_2(10.5 eV), CO(11.40 eV), and CO(11.52 eV) ones for which no radiative transitions are accounted for.

By also considering the 10.5 eV state of CO_2 as a dissociative one instead of a metastable state (see the dotted curves reported in Fig. 9), the resulting eedf at $t = 50$ ms is depleted at higher energy values ($\varepsilon \geq 10.5$ eV) with respect to the thin and thick case, while at $t = 100$ ms, it is further decreased by losing the peaks due to the CO_2(10.5 eV) state. It should also be noted that the repetition of the

plateaux in the eedf can be rationalized by using the "golden rule" developed by D'Ammando et al.[46]

A confirmation of the eedf's peaks behavior can be obtained by looking at Fig. 10, which shows the density time evolution of the most important electronic excited states affecting the eedf, i.e., the CO_2, CO, and O ones, in the optically thick and thin plasma conditions. By considering the CO_2(10.5 eV) electronic state as a metastable state, its concentration, governed only by the electron impact excitation/deexcitation processes, is independent of the thin and thick choice and remains more or less constant during the time evolution. For the CO system, in the thick plasma conditions, all the electronic excited states, with the only exception of CO(6 eV), increases their densities, reaching high concentrations and thus strongly affecting the eedf. The CO(6 eV), instead, decreases its density since it is quenched by the Porshnev process (V17 Table VI or Q1 Table VIII) thus explaining the corresponding CO(6 eV) peak's absence in the eedf (see Figs. 8(b) and 9). In thin conditions, instead, the population of the emitting CO electronic states (6.863 eV, 8.03 eV, 10.4 eV, and 10.78 eV) decreases and all their corresponding peaks in the eedf disappear, leaving only the peaks for CO(11.40 eV) and CO(11.52 eV) which do not decay radiatively. The concentration of the O electronic excited states [see Fig. 10(c)] is affected both by quenching processes (see Table VIII) and by radiation emission (see Table VII). In thick conditions, the main important peak is for the O(9.521 eV) electronic state, which is not subjected to any heavy-particle quenching process.
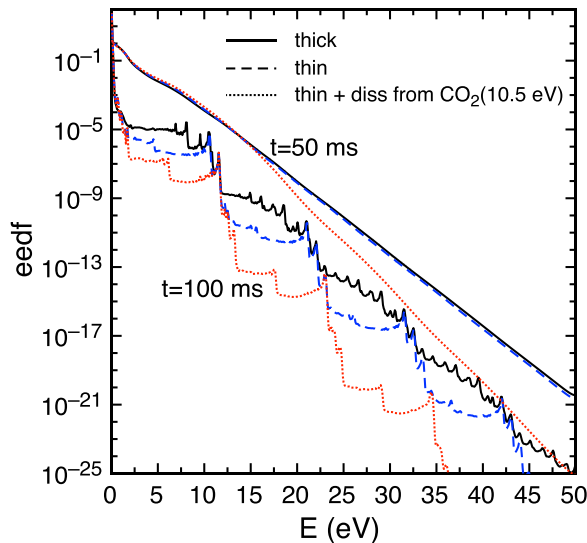
FIG. 9. Eedf at the end of the discharge ($t = 50$ ms) and of the post discharge ($t = 100$ ms) in the MW test case ($T_{gas} = 300$ K, $P = 20$ Torr, $P_d = 80$ W cm^{-3}, $t_{pulse} = 50$ ms, and $t_{pd} = 100$ ms) by considering an optically thick and thin plasma and by considering the CO_2 state (10.5 eV) as a dissociative one.

C. CO_2 and CO dissociation rates

In order to understand which are the main dissociation processes acting in the mixture, the heavy-particle dissociation rates (PVMs) are compared to electron impact ones, direct (DEM) and/or resonant (RES), both for CO_2 and CO. Such rates are calculated according to:

FIG. 10. (a) CO_2, (b) CO, and (c) O_2 electronic excited states density (EESD) time evolution in the thick and thin plasma conditions.

$$PVM_D(CO_2) = n_{tot} n_{CO_2} \sum_{v=0}^{v_{max}} K_D^{CO_2}(v) f_{CO_2}(v), \quad (6)$$

$$PVM_O(CO_2) = n_{CO_2} n_O \sum_{v=0}^{v_{max}} K_O^{CO_2}(v) f_{CO_2}(v), \quad (7)$$

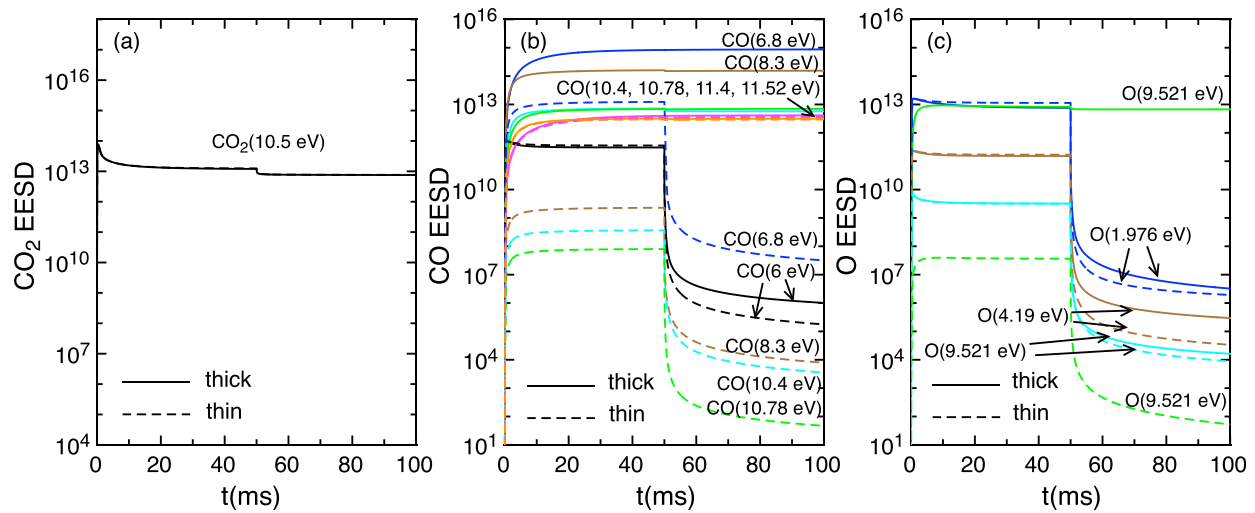$$DEM(CO_2) = n_e n_{CO_2} \sum_{v=0}^{v_{max}} K_{D_e}^{CO_2}(v) f_{CO_2}(v), \quad (8)$$

$$PVM_B(CO) = n_{CO}^2 \sum_{v=0}^{v_{max}} \sum_{w=0}^{w_{max}} K_B^{CO}(v,w) f_{CO}(v) f_{CO}(w), \quad (9)$$

$$PVM_D(CO) = n_{tot} n_{CO} \sum_{v=0}^{v_{max}} K_D^{CO}(v) f_{CO}(v), \quad (10)$$

$$DEM(CO) = n_e n_{CO} \sum_{v=0}^{v_{max}} K_{D_e}^{CO}(v) f_{CO}(v), \quad (11)$$

$$RES(CO) = n_e n_{CO} \sum_{v=0}^{v_{max}} K_{Res}^{CO}(v) f_{CO}(v), \quad (12)$$

where $f_{CO_2}(v)$ and $f_{CO}(v)$ are the CO_2 and CO vdf, $K_D^{CO_2}(v)$, and $K_O^{CO_2}(v)$ are the vibrational state selected rate coefficients for CO_2 dissociation by direct dissociation and by collision with O atoms, $K_B^{CO}(v,w)$ and $K_D^{CO}(v)$ are those for CO dissociation by Boudouard process and by direct dissociation, $K_{D_e}^{CO_2}(v)$ and $K_{D_e}^{CO}(v)$ for electron impact dissociation for CO_2 and CO, $K_{Res}^{CO}(v)$ for electron resonant collision for CO, and finally n_{CO_2}, n_{CO}, n_O, n_e, n_{tot} are the CO_2, CO, O, electron, and total number densities.

Figure 11 shows the time evolution of previous dissociation rates in the MW test case considered for (a) CO_2 and (b) CO in the optically thick plasma condition.

By looking at Fig. 11, it can be seen that, in the MW conditions, the dissociation induced by vibrational excitation prevails over the dissociation by electron impact during the discharge, indicating that the CO_2 and CO molecules dissociate using preferentially the

heavy-particle collisions and the vibrational excitation channel. Direct dissociation by heavy-particles for CO_2 and the Boudouard dissociation process for CO dominate the other mechanisms. In the post-discharge, the PVM rates reduce by several orders of magnitude due to the strong vdf deactivation, while DEM ones are still important due to the presence of a stationary non-equilibrium eedf with an over-populated tail characterized by several superelastic electronic peaks [Figs. 8(b) and 9].

D. Conversion and energy efficiency

A confirmation of the fact that, in the MW test case conditions of pressure and gas temperature, CO_2 dissociates essentially by using the vibrational excitation channel can also be obtained by looking at Fig. 12 in which the (a) CO_2 conversion rate ($X = 1 - \frac{n_{CO_2}(t_{pulse})}{n_{CO_2}(t_0)}$) and (b) its corresponding energy efficiency ($\eta = X \frac{2.9 \, eV}{SEI}$) are reported as a function of the specific energy input (SEI), in the same pressure and gas temperature conditions ($T_{gas} = 300$ K, P = 20 Torr), at t = 9.13 ms, at different power density values and by changing the electron impact dissociation cross section for CO_2. In particular, conversion results are reported by using the experimental Cosby cross section with threshold 11.6 eV and the Phelps cross section with threshold energy 7 eV. In the same figure, the comparison with the CO_2 conversion rates and energy efficiencies calculated by Kozák and Bogaerts[11] under the same conditions is also reported. As we can see, in these pressure and gas temperature conditions, the conversion values do not change with the choice of the electron impact cross sections (i.e., Cosby and/or Phelps).

Our calculated values are lower than those calculated[11] with a difference that increases with the power density. The discrepancy could be probably due to the different electron kinetic modules used in the two approaches.

A satisfactory agreement with the Berthelot and Bogaerts[24] results is obtained by comparing the stationary CO_2 vdf (see Fig. 13) calculated in MW test cases characterized by the same pressure
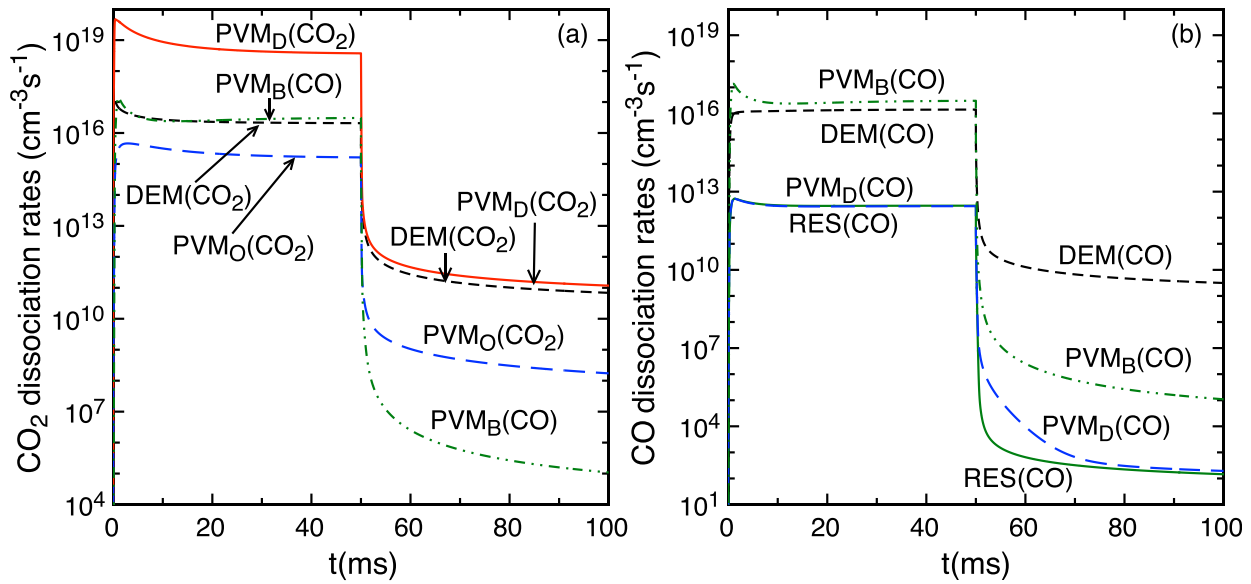
FIG. 11. (a) CO_2 and (b) CO dissociation rates in the MW test case ($T_{gas} = 300$ K, $P = 20$ Torr, $P_d = 80$ W cm^{-3}, $t_{pulse} = 50$ ms, $t_{pd} = 100$ ms, and optically thick plasma).

(P = 75 Torr) and different gas temperature and power densities,[24] with some differences in the highest energy part of the vdf tail. For this comparison, we have made sure to use the same rate coefficients for heavy-particle CO_2 dissociation processes as in Ref. 24, which are different from those used in Ref. 11. The stationary vdfs are obtained after 100 μs for the case at $T_{gas} = 300$ K and 1 μs for $T_{gas} = 2000$ K both in our calculations and in Ref. 24. A satisfactory agreement is also obtained for our calculated CO_2 vibrational and electron temperatures and electron densities, at $t = 100$ μs and $T_{gas} = 300$ K, at the two power densities, as reported in Table I.

E. Effect of gas temperature

In this section, the role of gas temperature in affecting the results will be investigated. Typical gas temperature values characterizing the MW plasma range between 2000 K and 3000 K, even if recent experiments on CO_2 MW discharges[47] have also measured larger values from 3500 K up to 5500 K. As a consequence, it is important to understand how the results depend on the gas temperature. The following Fig. 14 shows the comparison of CO_2, CO, and electron molar fractions calculated in the test case of Sec. III A ($T_{gas} = 300$ K, $P = 20$ Torr,
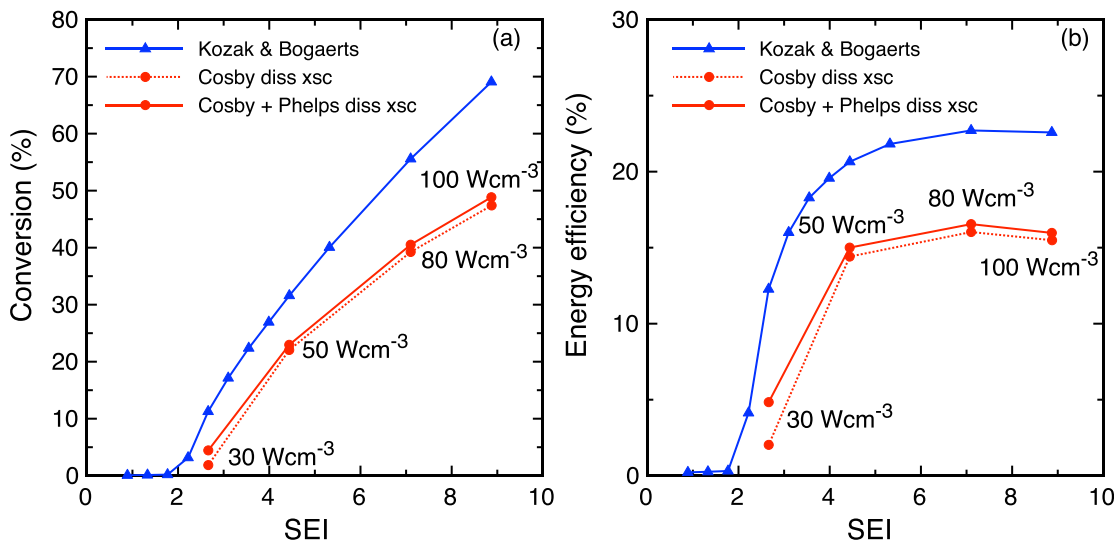
FIG. 12. (a) CO_2 conversion rates and (b) energy efficiency at $t = 9.13$ ms as a function of SEI, in the same pressure and gas temperature conditions ($T_{gas} = 300$ K, $P = 20$ Torr) but at different power density values and by changing the electron impact dissociation cross section for CO_2 (Cosby[28] and Cosby plus Phelps[25]). The corresponding calculated values by Kozak and Bogaerts[11] are reported for power densities of 10, 15, 20, 25, 30, 35, 40, 45, 50, 60, 80, and 100 W cm^{-3}.
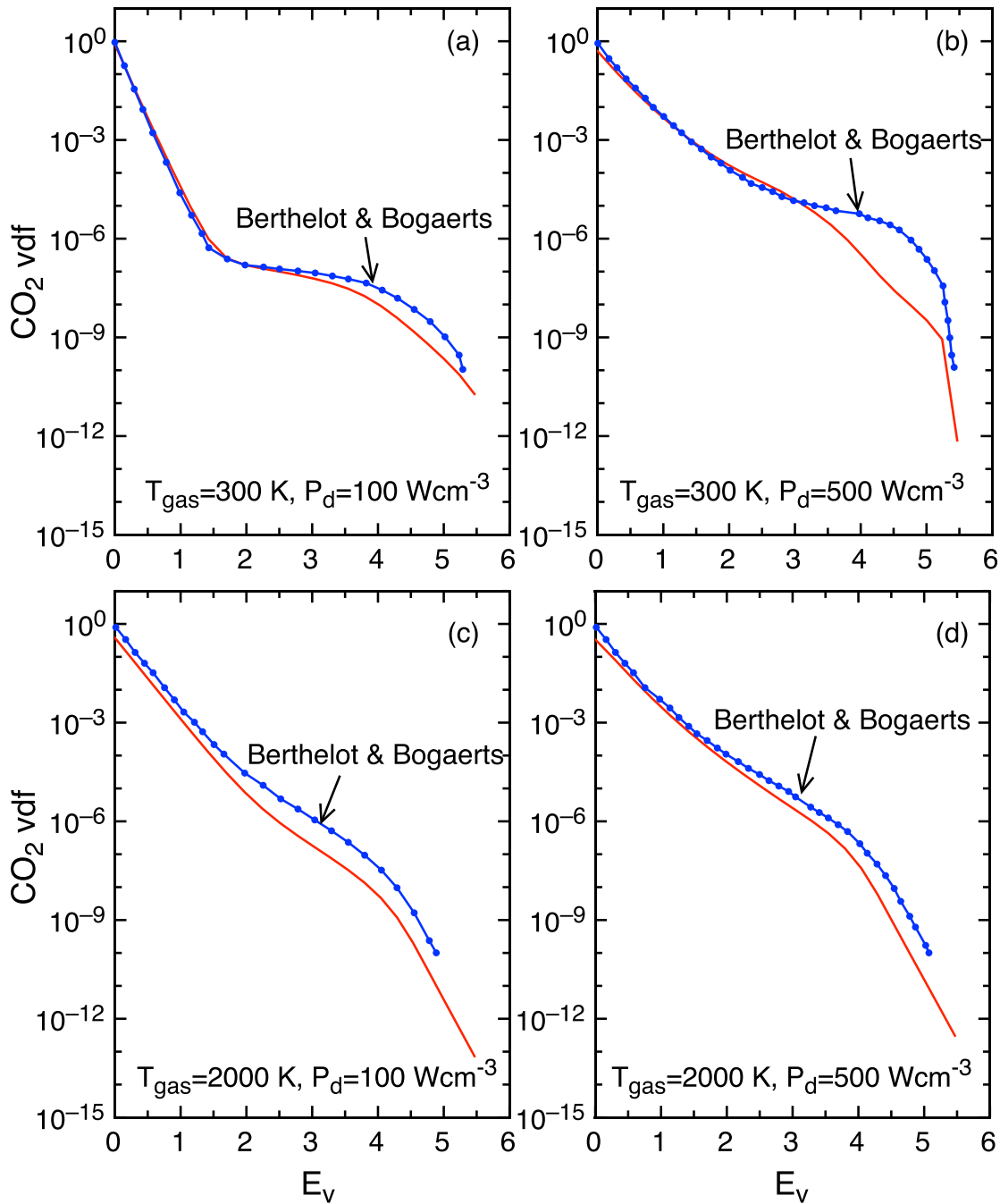
FIG. 13. Stationary vdf calculated at pressure $P = 75$ Torr, at different T_{gas} (300 K and 2000 K) and power density conditions P_d (100 W cm^{-3} and 500 W cm^{-3}) compared to the results of Berthelot and Bogaerts.[24]

$P_d = 80$ W cm^{-3}, $t_{pulse} = 50$ ms, $t_{pd} = 100$ ms, and optically thick) with those obtained by increasing the gas temperature ($T_{gas} = 2000$ K). At higher T_{gas}, the global behavior, however, depends also on the choice of the electron impact dissociation cross section used, i.e., Cosby or Phelps, showing, this time, the crucial role of this cross section in the CO_2 kinetics.

By considering the Cosby cross sections, the increase in T_{gas} reduces the CO_2 conversion into CO during the discharge (see Fig. 14), while with Phelps, the conversion is increased. Such behavior depends on the fact that by considering a high energy threshold dissociation cross section as a Cosby's one, the DEM mechanism has a lower importance in the kinetics and even if its contribution increases

TABLE I. Comparison of CO_2 vibrational, electron temperatures, and electron densities at $P = 75$ Torr, $T_{gas} = 300$ K, and at $t = 100$ μs.

	Berthelot and Bogaerts[24]		Our calculations	
	$P_d = 100$ Wcm^{-3}	$P_d = 500$ Wcm^{-3}	$P_d = 100$ Wcm^{-3}	$P_d = 500$ Wcm^{-3}
$T_v(t = 100$ μs)	1050 K	2120 K	1013 K	2000 K
$T_e(t = 100$ μs)	1.8 eV	1.8 eV	0.67 eV	1.8 eV
$n_e(t = 100$ μs)	2.3×10^{10} cm^{-3}	1.2×10^{11} cm^{-3}	6.8×10^{10} cm^{-3}	1.93×10^{11} cm^{-3}

by increasing T_{gas}, the overall kinetics in the studied T_{gas} range (300 K–2000 K) is dominated by the dissociation process induced by vibrational excitation, in particular the PVM$_D$ one. As already shown in the past,[16] such a PVM mechanism has a non-thermal behavior in this gas temperature range, i.e., the corresponding dissociation rate coefficient decreases with the increase in T_{gas}, thus explaining the observed decrease in CO_2 conversion with the increase in T_{gas}. This non-thermal behavior of the PVM$_D$ rates is due to the progressive elimination of overpopulated CO_2 vdf tails (V–V plateau) with the increase in T_{gas}.

By considering a lower threshold energy cross section as the Phelps's one, with the increase in T_{gas}, the overall kinetics passes through a regime in which the PVM mechanism dominates the kinetics to a regime in which the DEM mechanism starts prevailing, with a more thermal behavior of the discharge, i.e., the CO_2 conversion rate increases with T_{gas}.

Such explanation is confirmed by looking at Fig. 15 in which the DEM(CO_2), PVM$_D$(CO_2), and PVM$_O$(CO_2)

dissociation rates are shown as a function of time in the four cases investigated.

As it can be seen, passing from $T_{gas} = 300$ K to $T_{gas} = 2000$ K with the Cosby cross section, the DEM and PVM$_O$ rates increase, while the PVM$_D$ rate decreases during the discharge [Figs. 15(a) and 15(b)]. However, in both T_{gas} conditions, PVM$_D$ rate overcomes the other two. The different behaviors of the PVM$_O$ rate with respect to the PVM$_D$ one with the increase in T_{gas} are due to the fact that the PVM$_O$ rate is less dependent on the non-equilibrium shape of the highest energy part of the CO_2 vdf due to the lower value of the α coefficient used in the Fridman–Macheret model [see Eq. (3)] ($\alpha = 1$ for the PVM$_D$ and $\alpha = 0.5$ for the PVM$_O$, see Table V in the Appendix), i.e., a lower efficiency of the vibrational levels in lowering the dissociation activation barrier and enhancing the corresponding rate.

In the Phelps cross section case [Figs. 15(c) and 15(d)], instead, the PVM$_D$ rate overcomes the other dissociation mechanisms for $T_{gas} = 300$ K, while for $T_{gas} = 2000$ K, the DEM is greater than PVM$_D$
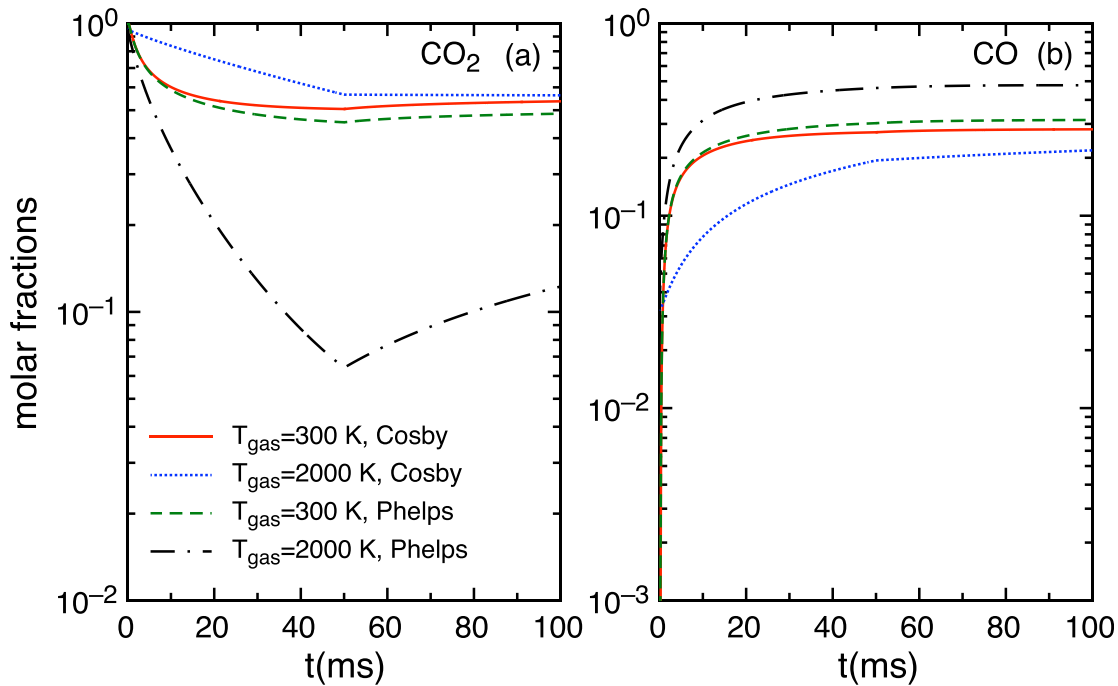
FIG. 14. (a) CO_2 and (b) CO molar fraction time evolution in the four test cases characterized by $P = 20$ Torr, $P_d = 80$ W cm^{-3}, $t_{pulse} = 50$ ms, $t_{pd} = 100$ ms, and different T_{gas} values (300 K–2000 K) and electron impact cross sections (Cosby and Phelps).
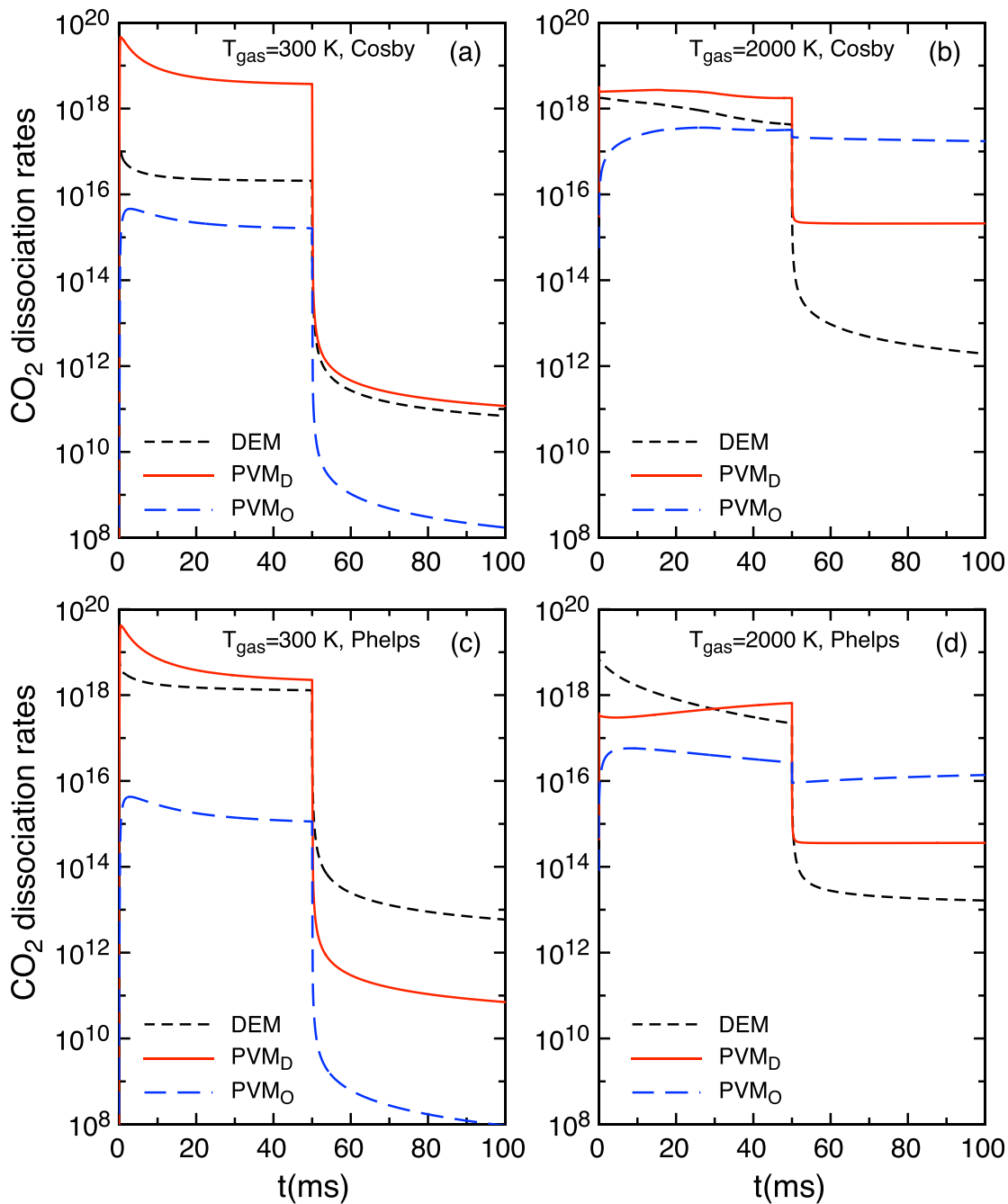
FIG. 15. CO_2 dissociation rates time evolution in four test cases characterized by $P = 20\,Torr$, $P_d = 80\,Wcm^{-3}$, $t_{pulse} = 50\,ms$, and different T_{gas} values (300 K–2000 K) and electron impact cross sections (Cosby and Phelps).

in the first part of the evolution (up to 30 ms), the reverse being true in the time range (30–50 ms).

The results in Figs. 14 and 15 give another confirmation that at a lower T_{gas}, the global behavior of the CO_2 plasma discharge is very little dependent on the choice of the electron impact cross section, as already shown in Fig. 12 by looking at the conversion and energy efficiency results. At $T_{gas} = 300\,K$, similar values for CO_2 and CO molar fractions (see Fig. 14) and PVM_D and PVM_O rates [see Figs. 15(a) and 15(c)] are obtained with the Cosby and the Phelps cross sections, with the only exception of the DEM rates, which increase passing from the Cosby to the Phelps cross sections, as a result of the integration of the eedf over a different threshold energy cross section.

IV. CONCLUSIONS AND PERSPECTIVES

The results reported in the present paper clearly show the importance of electronically excited states in the formation of eedf under different situations.

The results depend on the number of electronically excited states considered in each system which in the present work is rather limited for the CO_2, for which only one excited state at 10.5 eV has been considered, but larger for the CO, O, and C systems, formed during the dissociation of CO_2.

Very recently, Annaloro and Bultel (see Fig. 1 and Table I in Ref. 48) have improved the electronic excited level scheme of CO_2 by inserting three new triplet states with an energy of about 4 eV from the electronic ground state of CO_2. These new states can be important in affecting the eedf of the system in an energy range empty of electronic states. This effect could be compensated, however, by the presence of other components of the reacting CO_2 mixture with electronic energy of the order of 4 eV (see, for example, C and O atoms).

The present model based on the constancy of the power density injected in the plasma allows to investigate the behavior of the different plasma properties for times much longer than those obtained by the present authors using the E/N value. The constancy of the power density limits the variation of the electron molar fraction allowing a more interesting study of the kinetics as a function of time.

As already pointed out in our previous studies, the accuracy of the results depends on the choice of cross sections that in some cases becomes critical. As an example, despite the recent efforts made by Bogaerts et al.[26] and Grofulovic et al.,[27] the choice of the most appropriate electron impact dissociation cross section is still a problem that is yet to be solved. In our calculations, two different dissociation cross sections are used, with different threshold energies and different magnitudes, i.e., the experimental cross sections of Cosby and Helm and the Hake and Phelps ones. Our results have shown that at lower T_{gas}, i.e., 300 K, CO_2 conversion rate does not change by choosing different electron impact dissociation cross sections, since, in this condition, the heavy particle dissociation mechanism dominates the kinetics. At higher T_{gas}, i.e., 2000 K, instead, this choice becomes crucial.

Another point that should be more deeply investigated is the accuracy of heavy particle reaction rate coefficients, especially for the dependence of such coefficients on the vibrational quantum number, calculated here by using the semi-empirical method developed by Fridman.[10]

Moreover, the vibrational kinetics of the CO_2, CO, and O_2 systems should be coupled by V–V and V–T processes to correctly take into account vibrational energy exchanges between the systems. V–V transitions between CO_2 and CO are already included into the model, but V–V processes coupling CO_2–O_2 and CO–O_2 together with V–T processes of the kind CO–CO_2 and CO–O_2 in the CO vibrational kinetics and O_2–CO_2 and O_2–CO in the O_2 vibrational kinetics are not considered because of the poor knowledge of the corresponding rates. The neglect of previous V–V and V–T processes involving O_2, however, are expected not to have a strong impact on the overall kinetics in the test cases presented here due to the low O_2 concentration especially during the discharge.

Another point which should be improved concerns the quenching processes of the electronic excited states. In particular, it is very important in this case to understand the fraction of the energy lost in the quenching process going into the translational, rotational, and vibrational energy of the products. Particular attention should be devoted to the quenching of the $CO(a^3\Pi)$ metastable state,[20–22,45] which pumps all the electronic energy into the v = 27 vibrational level of CO, with large consequences on the CO vibrational distribution, i.e., a peak at v = 27, which is then smoothed by e–V and V–V processes.

Important improvements in the CO_2 vibrational structure are also needed. In the present work, we have used a complete description of the anharmonic asymmetric vibrational mode of CO_2 linked with weak interactions to the other two symmetric modes.[11,12] This approximation gives satisfactory results when compared with the experimental results of the dissociation of CO_2.

Other methods are nowadays proposed to consider a strong mixing of vibrational levels of the three modes of CO_2 which clearly is a better description of the vibrational levels. The method works very well for understanding CO_2 lasers or the vibrational distribution at low energy when it is confined to the low lying vibrational mixed levels. Interesting theoretical and experimental results in this direction have been recently presented by Silva et al.[49] and Klarenaar et al.[50]

On the other hand, for extending the method up to the dissociation limit of CO_2 as recently considered by Armenise and Kustova[51] and Kustova et al.,[52] one should consider thousand and thousand levels introducing in this case a practical impossibility to get reliable electron-molecule cross sections to be inserted in the Boltzmann equation. The last point has been recently discussed by Pietanza et al.[53] emphasizing the difficulty of the method also for low lying vibrational states of CO_2.

These difficulties are also present when using the Fokker Planck equation for describing the vibrational kinetics of CO_2.[54,55]

Another interesting approach has been recently proposed by Annaloro and Bultel[48] with the description of the CO_2 as an independent oscillator in the first levels up to a given threshold energy, and for higher energies, each vibrational modes up to the dissociation limit are considered with the other modes totally deactivated, i.e., $(v00)$, $(0v0)$, and $(00v)$.

Another important point to be defined is the role of the electronic state of CO_2 at 10.5 eV. In our approach, this state is assumed as a metastable state and its presence has large consequences on the eedf by creating peaks due to the corresponding superelastic electronic collisions. However, recently, Bogaerts et al.[26] have considered this state as a dissociative one. By making the same assumption, the 10.5 eV state is strongly depopulated and the resulting eedf strongly depletes due to the loss of the corresponding superelastic peaks.

Finally, CO_2 and other components such as CO radiate in the infrared range and this energy can be reabsorbed by the vdf distribution. Experimental and theoretical models based on the pumping of laser energy on the formed vibrational distribution of CO show that the existing plateau of CO is strongly altered by the arrival of laser photons (see Figs. 7.13 and 7.14 of Ref. 8). Thus, further improvements of the model should go in the direction to take into account the influence of reabsorbed infrared radiation on the vibrational kinetics.

In conclusion, despite the enormous efforts made by the international community, a complete understanding of CO_2 dissociation in plasma is still an open problem with several aspects that need further investigation and clarification.

APPENDIX: LIST OF ENERGY LEVELS AND REACTIONS

TABLE II. Vibrational levels for the ground electronic states of CO_2, CO, and O_2 molecules.

	$CO_2(X^1\Sigma_g^+)$	$CO(X^1\Sigma^+)$	$O_2(X^3\Sigma_g^-)$
Vibrational levels	$CO_2(00v)$, $v \leq 21$; $v_{b_1}(010)$ $v_{FL_1}(020) + (100)$ $v_{FL_2}(030) + (110)$ $v_{FL_3}(040) + (120)$ $+(200)$	$CO(v)$, $v \leq 80$	$O_2(v)$, $v \leq 34$

TABLE III. Electronic excited states for CO_2, CO, and O_2 and ground and electronic excited states for C and O.

Electronic excited states	Energy (eV)
$CO_2(10.5\,eV)$	10.5
$CO(a^3\Pi)$	6.0
$CO(a'^3\Sigma^+)$	6.863
$CO(A^1\Pi)$	8.03
$CO(b^3\Sigma^+)$	10.4
$CO(B^1\Sigma^+)$	10.78
$CO(C^1\Sigma^+)$	11.40
$CO(E^1\Sigma^+)$	11.52
$O_2(a^1\Delta_g)$	0.976
$O_2(b^1\Sigma_g^+)$	1.627
$C(^3P)$	0
$C(^1D)$	1.263
$C(^1S)$	2.684
$C(^5S)$	4.182
$O(^3P)$	0
$O(^1D)$	1.976
$O(^1S)$	4.19
$O(^3S^0)$	9.146
$O(^5S^0)$	9.521

TABLE IV. Electron impact reactions entering as cross sections in the electron Boltzmann code.

		References	Vibr. Levels
(X1)	$e + CO_2 \leftrightarrow e + CO_2$	56	
(X2)	$e + CO_2(000) \leftrightarrow e + CO_2(x)$, $x = v_{b_1}, v_{FL_i}$	25	
(X3)	$e + CO_2(00v) \leftrightarrow e + CO_2(00\omega)$	25[a]	
(X4)	$e + CO_2(000) \leftrightarrow e + CO_2(10.5\,eV)$	25	
(X5)	$e + CO_2(00v) \leftrightarrow e + e + CO_2^+$	25[b]	
(X6)	$e + CO_2(00v) \leftrightarrow e + C + O$	25,28[b]	
(X7)	$e + CO \leftrightarrow e + CO$	29	

TABLE IV. (Continued.)

		References	Vibr. Levels
(X8)	$e + CO(v) \rightarrow CO^-(^2\Pi)$ $\rightarrow e + CO(w)$	31	$v, w = 0 - 80$
(X9)	$e + CO(v) \rightarrow CO^-(^2\Pi)$ $\rightarrow e + C(^3P) + O(^3P)$	32	$v = 0 - 80$
(X10)	$e + CO(v) \rightarrow CO^-(X^2\Pi)$ $\rightarrow C(^3P) + O^-(^2P)$	32	$v = 0 - 80$
(X11)	$e + CO(v=0) \rightarrow CO^-(A^2\Sigma, ..)$ $\rightarrow C(^3P) + O^-(^2P)$	57	
(X12)	$C(^3P) + O^-(^2P)$ $\rightarrow e + CO(v=0)$	58	
(X13)	$e + CO(v) \leftrightarrow e + e + CO^+$	29[b]	
(X14)	$e + CO(0) \leftrightarrow e + CO(X)$, $X = a^3\Pi, a'^3\Sigma^+, b^3\Sigma^+, A^1\Pi,$ $B^1\Sigma^+, C^1\Sigma^+, E^1\Sigma^+$	29	
(X15)	$e + CO(v) \leftrightarrow e + C + O$	30[b]	
(X16)	$e + O_2 \leftrightarrow e + O_2$	59	
(X17)	$e + O_2(v) \rightarrow O_2^-(^2\Pi_g, ^2\Pi_u, ^4\Sigma_u^-, ^2\Sigma_u^-) \rightarrow e + O_2(w)$	33	$v, w = 0 - 41$
(X18)	$e + O_2(v) \rightarrow O_2^{-*} \rightarrow e + 2O(^3P)$	34	$v = 0 - 41$
(X19)	$e + O_2(v) \rightarrow e + O_2^*(A^3\Sigma_u^+)$ $\rightarrow O(^3P) + O(^3P) + e$	35	$v = 0, 1, 2$
(X20)	$e + O_2(v) \rightarrow e + O_2^*(B^3\Sigma_u^-)$ $\rightarrow O(^3P) + O(^1D) + e$	36	$v = 0 - 30$
(X21)	$e + O_2(v) \rightarrow e + O_2^*(B^3\Sigma_u^-)$ $\rightarrow O(^3P) + O(^3P) + e$	36	$v = 0 - 30$
(X22)	$e + O_2(v) \rightarrow 2e + O_2^+$	37	$v = 0 - 32$
(X23)	$e + O_2(X^3\Sigma_g^-; v) \rightarrow O_2^{-*}$ $\rightarrow O^-(^2P) + O(^3P)$	34	$v = 0 - 41$
(X24)	$e + O_2(v=0) \rightarrow e + O_2(a^1\Delta_g)$	59	
(X25)	$e + O_2(v=0) \rightarrow e + O_2(b^1\Sigma_g^+)$	59	
(X26)	$e + O_2(a^1\Delta_g)$ $\rightarrow O^-(^2P) + O(^3P)$	59	
(X27)	$e + O_2(b^1\Sigma_g^+)$ $\rightarrow O^-(^2P) + O(^3P)$	59	
(X28)	$e + C \leftrightarrow e + C$	60	
(X29)	$e + C(^3P) \leftrightarrow e + C^+$	60	
(X30)	$e + C(^3P) \leftrightarrow e + C(X)$, $X = {}^1D, {}^1S, {}^5S^0$	60	
(X31)	$e + O \leftrightarrow e + O$	61	
(X32)	$e + O(^3P) \leftrightarrow e + O^+$	61	
(X33)	$e + O(^3P) \leftrightarrow e + O(X)$, $X = {}^1D, {}^1S, {}^5S^0, {}^3S^0$	61	

[a]Fridman scaling law [see Eq. (1)].
[b]Threshold shifting [see Eq. (2)].

TABLE V. Heavy-particle chemical processes.

		References	α
(H1)	$CO_2(00v) + M \rightarrow CO + O + M$	11[a]	1
(H2)	$CO_2(00v) + O \rightarrow CO + O_2$	11[a]	0.5
(H3)	$CO + O + M \rightarrow CO_2 + M$	11	
(H4)	$CO(v) + O_2 \rightarrow CO_2 + O$	11[a]	0.5
(H5)	$e + CO_2^+ \rightarrow CO + O$	11	
(H6)	$CO(v) + M \rightarrow C + O + M$	62	
(H7)	$CO(v) + CO(w) \rightarrow CO_2 + C$	38,40	
(H8)	$C + O + M \rightarrow CO + M$	11	
(H9)	$CO^+ + e \rightarrow C + O$	11	
(H10)	$O_2(v) + O \leftrightarrow 2O + O$	63	
(H11)	$O_2(v) + O_2 \leftrightarrow 2O + O_2$	41	

[a]Fridman–Macheret α model.[10]

TABLE VI. Vibrational kinetic processes.

		References
(V1)	$CO_2(v_{b_1}) + M \rightarrow CO_2(000) + M$	11
(V2)	$CO_2(001) + M \rightarrow CO_2(v_{b_1}) + M$	11
(V3)	$CO_2(001) + M \rightarrow CO_2(v_{FL_1}) + M$	11
(V4)	$CO_2(001) + M \rightarrow CO_2(v_{FL_2}) + M$	11
(V5)	$CO_2(001) + CO_2(000) \rightarrow CO_2(000) + CO_2(001)$	11
(V6)	$CO_2(001) + CO_2(000) \rightarrow CO_2(v_{FL_1}) + CO_2(v_{b_1})$	11
(V7)	$CO_2(001) + CO_2(000) \rightarrow CO_2(v_{b_1}) + CO_2(v_{FL_1})$	11
(V8)	$CO_2(00v) + M \rightarrow CO_2(00v-1) + M$	11[a]
(V9)	$CO_2(00v) + CO_2(00w)$ $\rightarrow CO_2(00v-1) + CO_2(00w+1)$	11[a]
(V10)	$CO_2(00v) + CO_2(000)$ $\rightarrow CO_2(00v-1) + CO_2(v_{FL_1}, v_{b_1})$	11[a]
	CO_2–CO	
(V11)	$CO_2(00v) + CO(w-1)$ $\rightarrow CO_2(00v-1) + CO(w)$	11[a]
(V12)	$CO(v) + CO(w-k) \rightarrow CO(v-k) + CO(w)$	43,64,65
(V13)	$CO(v) + CO \rightarrow CO(v-k) + CO$	43,64,65
(V14)	$CO(v) + C \rightarrow CO(v-1) + C$	44
(V15)	$CO(v) + O \rightarrow CO(v-1) + O$	44
(V16)	$CO(v) \rightarrow CO(v-1) + h\nu$	66
(V17)	$CO(a^3\Pi, w=0) + CO \rightarrow CO(v=27) + CO$	45
(V18)	$O_2(v+1) + O_2(w) \rightarrow O_2(v) + O_2(w+1)$	67
(V19)	$O_2(v) + O \rightarrow O_2(w) + O$	63
(V20)	$O_2(v) + O_2 \rightarrow O_2(v-1) + O_2$	67

[a]SSH scaling law.[42]

TABLE VII. Electronic excited states optical transitions.

		A (s^{-1})[68,69]
(E1)	$CO(a'^3\Sigma^+) \rightarrow CO(a^3\Pi) + h\nu$	10^4
(E2)	$CO(A^1\Pi) \rightarrow CO(X^1\Sigma^+) + h\nu$	10^8

TABLE VII. (*Continued.*)

		A (s^{-1})[68,69]
(E3)	$CO(b^3\Sigma^+) \rightarrow CO(a^3\Pi) + h\nu$	1.8518×10^7
(E4)	$CO(B^1\Sigma^+) \rightarrow CO(X^1\Sigma^+) + h\nu$	1.063×10^7
(E5)	$CO(B^1\Sigma^+) \rightarrow CO(A^1\Pi) + h\nu$	2.0×10^7
(E6)	$O(^3S) \rightarrow O(^3P) + h\nu$	6.116×10^8
(E7)	$O(^3S) \rightarrow O(^1D) + h\nu$	1.83×10^3
(E8)	$O(^3S) \rightarrow O(^1S) + h\nu$	4.61
(E9)	$O(^5S) \rightarrow O(^1D) + h\nu$	5.32×10^{-3}
(E10)	$O(^5S) \rightarrow O(^3P) + h\nu$	5.56×10^3
(E11)	$O(^1S) \rightarrow O(^3P) + h\nu$	7.5642×10^{-2}
(E12)	$O(^1S) \rightarrow O(^1D) + h\nu$	1.26
(E13)	$O(^1D) \rightarrow O(^3P) + h\nu$	7.47535×10^{-3}
(E14)	$C(^1S) \rightarrow C(^3P) + h\nu$	2.32×10^{-3}
(E15)	$C(^1S) \rightarrow C(^1D) + h\nu$	5.99×10^{-1}
(E16)	$C(^5S) \rightarrow C(^3P) + h\nu$	29.6

TABLE VIII. Electronic excited states quenching channels.

		References
(Q1)	$CO(a^3\Pi, w=0) + CO \rightarrow CO(v=27) + CO$	45
(Q2)	$O(^1D) + O(^3P) \rightarrow O(^3P) + O(^3P)$	70–72
(Q3)	$O(^1S) + O(^3P) \rightarrow O(^1D) + O(^1D)$	70–72
(Q4)	$O(^5S) + O(^3P) \rightarrow O(^3P) + O(^3P)$	73
(Q5)	$C(^1D) + CO \rightarrow C(^3P) + CO$	74
(Q6)	$C(^1S) + CO \rightarrow C(^3P) + CO$	74
(Q7)	$C(^5S) + C(^3P) \rightarrow C(^3P) + C(^3P)$	74
(Q8)	$O_2(a^1\Delta_g) + O(0) \leftrightarrow O_2(0) + O(0)$	70
(Q9)	$O_2(a^1\Delta_g) + O_2(0) \leftrightarrow O_2(0) + O_2(0)$	70
(Q10)	$O_2(a^1\Delta_g) + O_2(a^1\Delta_g) \leftrightarrow O_2(b^1\Sigma_g^+) + O_2(0)$	70
(Q11)	$O_2(b^1\Sigma_g^+) + O(0) \leftrightarrow O_2(a^1\Delta_g) + O(0)$	70
(Q12)	$O_2(b^1\Sigma_g^+) + O_2(0) \leftrightarrow O_2(a^1\Delta_g) + O_2(0)$	70
(Q13)	$O_2(b^1\Sigma_g^+) + O(0) \leftrightarrow O_2(0) + O(^1D)$	70

REFERENCES

[1]J. Bretagne, G. Delouya, C. Gorse, M. Capitelli, and M. Bacal, "Electron energy distribution functions in electron-beam-sustained discharges: Application to Manetic Multicusp hydrogen discharges," J. Phys. D **18**, 811–825 (1985).

[2]K. Hassouni, A. Gicquel, and M. Capitelli, "The role of dissociative attachment from Rydberg states in enhancing H-concentration in moderate- and low-pressure H$_2$ plasma sources," Chem. Phys. Lett. **290**, 502–508 (1998).

[3]K. Hassouni, A. Gicquel, M. Capitelli, and J. Loureiro, "Chemical kinetics and energy transfer in moderate pressure H$_2$ plasmas used in diamond MPACVD processes," Plasma Sources Sci. Technol. **8**, 494–512 (1999).

[4]M. Capitelli, M. Cacciatore, R. Celiberto, O. D. Pascale, P. Diomede, F. Esposito, A. Gicquel, C. Gorse, K. Hassouni, A. Laricchiuta, S. Longo, D. Pagano, and M. Rutigliano, "Vibrational kinetics, electron dynamics and elementary processes in H$_2$ and D$_2$ plasmas for negative ion production: Modelling aspects," Nucl. Fusion **46**(6), S260–S274 (2006).

[5]G. Colonna, L. D. Pietanza, G. D'Ammando, R. Celiberto, M. Capitelli, and A. Laricchiuta, "Vibrational kinetics of electronically excited states in H_2 discharges," Eur. Phys. J. D **71**(11), 279 (2017).

[6]M. Capitelli, G. Colonna, G. D'Ammando, V. Laporta, and A. Laricchiuta, "The role of electron scattering with vibrationally excited nitrogen molecules on non-equilibrium plasma kinetics," Phys. Plasmas **20**, 101609 (2013).

[7]A. Annusova, D. Marinov, J.-P. Booth, N. Sirse, M. L. Da Silva, B. Lopez, and V. Guerra, "Kinetics of highly vibrationally excited $O_2(X)$ molecules in inductively-coupled oxygen plasmas," Plasma Sources Sci. Technol. **27**, 045006 (2018).

[8]M. Capitelli, R. Celiberto, G. Colonna, F. Esposito, C. Gorse, K. Hassouni, A. Laricchiuta, and S. Longo, *Fundamental Aspects of Plasma Chemical Physics: Kinetics* Springer Series in Atomic, Optical and Plasma Physics Vol. 85 (Springer, New York, 2016).

[9]M. Capitelli and L. D. Pietanza, "Past and present aspects of Italian plasma chemistry," Rendiconti Lincei Sci. Fis. Nat. **30**, 31–48 (2019).

[10]A. Fridman, *Plasma Chemistry* (Cambridge University Press, UK, 2012).

[11]T. Kozák and A. Bogaerts, "Splitting of CO_2 by vibrational excitation in non-equilibrium plasmas: A reaction kinetics model," Plasma Sources Sci. Technol. **23**, 045004 (2014).

[12]T. Kozák and A. Bogaerts, "Evaluation of the energy efficiency of CO_2 conversion in microwave discharges using a reaction kinetics model," Plasma Sources Sci. Technol. **24**, 015024 (2014).

[13]A. Bogaerts, T. Kozák, K. van Laer, and R. Snoeckx, "Plasma-based conversion of CO_2: Current status and future challenges," Faraday Discuss. **183**, 217 (2015).

[14]R. Aerts, W. Somers, and A. Bogaerts, "Carbon dioxide splitting in a dielectric barrier discharge plasma: A combined experimental and computational study," ChemSusChem **8**, 702 (2015).

[15]L. D. Pietanza, G. Colonna, G. D'Ammando, and M. Capitelli, "Time-dependent coupling of electron energy distribution function, vibrational kinetics of the asymmetric mode of CO_2 and dissociation, ionization and electronic excitation kinetics under discharge," Plasma Phys. Controlled Fusion **59**, 014035 (2017).

[16]M. Capitelli, G. Colonna, G. D'Ammando, and L. D. Pietanza, "Self-consistent time dependent vibrational and free electron kinetics for CO_2 dissociation and ionization in cold plasmas," Plasma Sources Sci. Technol. **26**, 055009 (2017).

[17]M. Capitelli, G. Colonna, G. D'Ammando, K. Hassouni, A. Laricchiuta, and L. D. Pietanza, "Coupling of plasma chemistry, vibrational kinetics, collisional-radiative models and electron energy distribution function under non-equilibrium conditions," Plasma Process. Polym. **14**, 1600109 (2017).

[18]L. D. Pietanza, G. Colonna, G. D'Ammando, A. Laricchiuta, and M. Capitelli, "Vibrational excitation and dissociation mechanisms of CO_2 under non-equilibrium discharge and post-discharge conditions," Plasma Sources Sci. Technol. **24**, 042002 (2015).

[19]L. D. Pietanza, G. Colonna, G. D'Ammando, A. Laricchiuta, and M. Capitelli, "Electron energy distribution functions and fractional power transfer in "cold" and excited CO_2 discharge and post-discharge," Phys. Plasmas **23**, 013515 (2016).

[20]L. D. Pietanza, G. Colonna, and M. Capitelli, "Non-equilibrium plasma kinetics of reacting CO: An improved state to state approach," Plasma Sources Sci. Technol. **26**, 125007 (2017).

[21]L. D. Pietanza, G. Colonna, and M. Capitelli, "Non-equilibrium electron and vibrational distributions under nanosecond repetitively pulsed CO discharges and afterglows: I. optically thick plasmas," Plasma Sources Sci. Technol. **27**, 095004 (2018).

[22]L. D. Pietanza, G. Colonna, and M. Capitelli, "Non-equilibrium electron and vibrational distributions under nanosecond repetitively pulsed CO discharges and afterglows: II. the role of radiative and quenching processes," Plasma Sources Sci. Technol. **27**, 095003 (2018).

[23]G. D'Ammando, M. Capitelli, F. Esposito, A. Laricchiuta, L. D. Pietanza, and G. Colonna, "The role of radiative reabsorption on the electron energy distribution functions in H_2/He plasma expansion through a tapered nozzle," Phys. Plasmas **21**, 093508 (2014).

[24]A. Berthelot and A. Bogaerts, "Modeling of CO_2 splitting in a microwave plasma: How to improve the conversion and energy efficiency," J. Phys. Chem. C **121**(15), 8236–8251 (2017).

[25]R. D. Hake and A. V. Phelps, "Momentum-transfer and inelastic-collision cross sections for electrons in O_2, CO, and CO_2," Phys. Rev. **158**, 70 (1967).

[26]A. Bogaerts, W. Wang, A. Berthelot, and V. Guerra, "Modeling plasma-based CO_2 conversion: Crucial role of the dissociation cross section," Plasma Sources Sci. Technol. **25**, 055016 (2016).

[27]M. Grofulovic, L. L. Alves, and V. Guerra, "Electron-neutral scattering cross sections for CO_2: A complete and consistent set and an assessment of dissociation," J. Phys. D: Appl. Phys **49**(39), 39527 (2016).

[28]P. C. Cosby and H. Helm, "Dissociation rates of diatomic molecules," Report No. AD-A266 464 WL-TR-93-2004 (Wright-Patterson Airforce Base, Dayton, OH, 1993).

[29]Y. Itikawa, "Cross sections for electron collisions with carbon monoxide," J. Phys. Chem. Ref. Data **44**, 013105 (2015).

[30]P. C. Cosby, "Electron-impact dissociation of carbon monoxide," J. Chem. Phys. **98**, 7804 (1993).

[31]V. Laporta, C. M. Cassidy, J. Tennyson, and R. Celiberto, "Electron-impact resonant vibration excitation cross sections and rate coefficients for carbon monoxide," Plasma Sources Sci. Technol. **21**, 045005 (2012).

[32]V. Laporta, J. Tennyson, and R. Celiberto, "Carbon monoxide dissociative attachment and resonant dissociation by electron-impact," Plasma Sources Sci. Technol. **25**, 01LT04 (2016).

[33]V. Laporta, R. Celiberto, and J. Tennyson, "Resonant vibrational-excitation cross sections and rate constants for low-energy electron scattering by molecular oxygen," Plasma Sources Sci. Technol. **22**, 025001 (2013).

[34]V. Laporta, R. Celiberto, and J. Tennyson, "Dissociative electron attachment and electron-impact resonant dissociation of vibrationally excited O_2 molecules," Phys. Rev. A **91**, 012701 (2015).

[35]M. Capitelli and R. Celiberto, "Electron-molecule cross sections for plasma applications: The role of internal energy of the target," in *Novel Aspects of Electron-Molecule Collisions*, edited by K. H. Becker (World Scientific, Singapore, 1998), pp. 283–323.

[36]A. Laricchiuta, R. Celiberto, and M. Capitelli, "Electron impact cross-sections for electronic excitation of vibrationally excited O_2 to $B^3\Sigma_u^-$ state," Chem. Phys. Lett. **329**, 526–532 (2000).

[37]A. V. Kosarim, B. M. Smirnov, M. Capitelli, A. Laricchiuta, and F. Paniccia, "Electron impact ionization cross sections of vibrationally and electronically excited oxygen molecules," Chem. Phys. Lett. **422**, 513–517 (2006).

[38]P. R. Barreto, H. de, O. Euclides, A. F. Albernaz, V. Aquilanti, M. Capitelli, G. Grossi, A. Lombardi, S. Macheret, and F. Palazzetti, "Gas phase Boudouard reactions involving singlet-singlet and singlet-triplet CO vibrationally excited states: Implications for the non-equilibrium vibrational kinetics of CO/CO_2 plasmas," Eur. Phys. J. D **71**, 259 (2017).

[39]V. D. Rusanov, A. A. Fridman, and S. V. Sholin, "The effect of non-Boltzmann population of vibrationally excited states on the carbon reduction in a nonequilibrium plasma," Sov. Phys. Dokl. **22**, 757 (1977).

[40]K. A. Essenigh, Y. G. Utkin, C. Bernard, I. V. Adamovich, and J. W. Rich, "Gas phase Boudouard disproportionation reaction between highly vibrationally excited CO molecules," Chem. Phys. **330**, 506–514 (2006).

[41]M. Cacciatore, M. Capitelli, and M. Dilonardo, "Non equilibrium vibrational population and dissociation rates of oxygen in electrical discharges—The role of atoms and of the recombination process," Beitr. Plasmaphy. **18**(5), 279–299 (1978).

[42]R. N. Schwartz, Z. I. Slawsky, and K. F. Herzfeld, "Calculation of vibrational relaxation times in gases," J. Chem. Phys. **20**, 1591 (1952).

[43]I. V. Adamovich, S. O. Macheret, J. W. Rich, and C. E. Treanor, "Vibrational energy transfer rates using a forced harmonic oscillator model," J. Therm. Heat Transfer **12**, 57–65 (1998).

[44]U. Schmailzl and M. Capitelli, "Nonequilibrium dissociation of CO induced by electron-vibration and IR-laser pumping," Chem. Phys. **41**, 143–151 (1979).

[45]P. I. Porshnev, H. L. Wallaart, M. Y. Perrin, and J. P. Martin, "Modeling of optical pumping experiments in CO. I. Time-resolved experiments," Chem. Phys. **213**, 111–122 (1996).

[46]G. D'Ammando, G. Colonna, M. Capitelli, and A. Laricchiuta, "Superelastic collisions under low temperature plasma and afterglow conditions: A golden rule to estimate their quantitative effects," Phys. Plasmas **22**(3), 034501 (2015).

[47]P. W. C. Groen, A. J. Wolf, T. W. H. Righart, M. C. M. v de Danden, F. J. J. Peeters, and W. A. Bongers, "Numerical model for the determination of the

reduced electric field in a CO_2 microwave plasma derived by the principle of impedance matching," Plasma Sources Sci. Technol. **28**(7), 075016 (2019).

[48]J. Annaloro and A. Bultel, "Vibrational and electronic collisional-radiative model in CO_2-N_2-Ar mixtures for Mars entry problems," Phys. Plasmas **26**, 103505 (2019).

[49]T. Silva, M. Grofulovic, L. Terraz, C. D. Pintassilgo, and V. Guerra, "Modelling the input and relaxation of vibrational energy in CO_2 plasmas," J. Phys. D: Appl. Phys. **51**, 464001 (2018).

[50]B. L. M. Klarenaar, R. Engel, D. C. M. van de Bekerom, M. C. M. van de Sanden, A. S. Morillo-Candas, and O. Guaitella, "Time evolution of vibrational temperatures in a CO_2 glow discharge measured with infrared absorption spectroscopy," Plasma Sources Sci. Technol. **26**, 115008 (2017).

[51]I. Armenise and E. Kustova, "Effect of asymmetric mode on CO_2 state-to-state vibrational_chemical kinetics," J. Phys. Chem. A **122**(4), 8709–8721 (2018).

[52]E. V. Kustova, E. A. Nagnibeda, and I. Armenise, "Vibrational-chemical kinetics in Mars Entry Problems," Open Plasma Phys. J. **7**(1), 76–87 (2014).

[53]L. D. Pietanza, G. Colonna, V. Laporta, R. Celiberto, G. D'Ammando, and A. Laricchiuta, "Influence of electron molecule resonant vibrational collisions over the symmetric mode and direct excitation-dissociation cross sections of CO_2 on the electron energy distribution function and dissociation mechanisms in cold pure CO_2 plasmas," J. Phys. Chem. A **120**, 2614–2628 (2016).

[54]P. Diomede, M. C. M. Van De Sanden, and S. Longo, "Insight into CO_2 dissociation in plasma from numerical solution of a vibrational diffusion equation," J. Phys. Chem. C **121**(36), 19568–19576 (2017).

[55]P. Viegas, M. C. M. Van De Sanden, S. Longo, and P. Diomede, "Validation of the Fokker-Planck approach to vibrational kinetics in CO_2 plasma," J. Phys. Chem. C **123**(37), 22823–22831 (2019).

[56]Y. Itikawa, "Cross sections for electron collisions with carbon dioxide," J. Phys. Chem. Ref. Data **31**, 749 (2002).

[57]D. Rapp and D. D. Briglia, "Total cross sections for ionization and attachment in gases by electron impact. II. Negative-ion formation," J. Chem. Phys. **43**, 1480 (1965).

[58]F. C. Fehsenfeld, E. E. Ferguson, and A. L. Schmeltekopf, "Thermal-energy associative-detachment reactions of negative ions," J. Chem. Phys. **45**, 1844 (1966).

[59]A. A. Ionin, A. P. Napartovich, and N. N. Yuryshev, "Physics and engineering of singlet delta oxygen production in low-temperature plasma," J. Phys. D: Appl. Phys. **40**, R25–R61 (2007).

[60]Y. Wang, O. Zatsarinny, and K. Bartschat, "B-spline R-matrix-with pseudostates calculations for electron-impact excitation and ionization of carbon," Phys. Rev. A **87**, 012704 (2013).

[61]R. R. Laher and F. R. Gilmor, "Updated excitation and ionization cross sections for electron impact on atomic oxygen," J. Phys. Chem. Ref. Data **19**, 277 (1990).

[62]R. L. Macdonald, A. Munafò, C. O. Johnston, and M. Panesi, "Nonequilibrium radiation and dissociation of CO molecules in shock-heated flows," Phys. Rev. Fluids **1**, 043401 (2016).

[63]F. Esposito, I. Armenise, G. Capitta, and M. Capitelli, "O-O_2 state-to-state vibrational relaxation and dissociation rates based on quasiclassical calculations," Chem. Phys. **351**, 91–98 (2008).

[64]E. Plonjes, P. Palm, A. P. Chernukho, I. V. Adamovich, and J. W. Rich, "Time-resolved Fourier transform infrared spectroscopy of optically pumped carbon monoxide," Chem. Phys. **256**, 315–331 (2000).

[65]M. Cacciatore and G. D. Billing, "Semiclassical calculation of VV and VT rate coefficients in CO," Chem. Phys. **58**, 395–407 (1981).

[66]S. R. Langhoff and C. W. Bauschlicher, Jr., "Global dipole moment function for the $X^1\Sigma^+$ ground state of CO," J. Chem. Phys. **102**, 5220–5225 (1995).

[67]G. D. Billing and R. E. Kolesnick, "Vibrational relaxation of oxygen. State to state rate constant," Chem. Phys. Lett. **200**, 382–386 (1992).

[68]A. Bultel, I. F. Schneider, and Y. Babou, "CO and C_2 excited states relaxation in CO_2 plasmas derived from a collisional-radiative model," J. Phys. Conf. Ser. **511**, 012059 (2014).

[69]A. Kramida, Yu. Ralchenko, J. Reader, and NIST ASD Team, NIST Atomic Spectra Database (version 5.7.1) (National Institute of Standards and Technology, Gaithersburg, MD, 2019), available at https://physics.nist.gov/asd.

[70]M. Capitelli, C. M. Ferreira, B. F. Gordiets, and A. I. Osipov, *Plasma Kinetics in Atmospheric Gases* (Springer, 2000).

[71]V. J. Abreu, J. H. Yee, S. C. Solomon, and A. Dalgarno, "The quenching rate of $O(^1D)$ by $O(^3P)$," Planet. Space Sci. **34**, 1143 (1986).

[72]T. G. Slanger and G. Black, "Quenching of $N(^2D)$ by N_2 and H_2O," J. Chem. Phys. **64**, 3763 (1976).

[73]A. M. Diamy, N. Gonzalez-Flesca, and J. C. Legrand, "Formation et desactivation par l'oxygene moleculaire de l'atome metastable $O(^5S)$ dans une decharge oxygene-helium," Spectrochim. Acta B **41**(4), 317–325 (1986).

[74]R. J. Donovan and D. Husain, "Recent advances in the chemistry of electronically excited atoms," Chem. Rev. **70**, 489–516 (1970).